

Interpretability of Multivariate Brain Maps in Brain Decoding: Definition and Quantification

Seyed Mostafa Kia^{1,2,3,*}

Center for Mind/Brain Sciences (CIMeC), University of Trento, via delle Regole 101, 38123, Mattarello, TN, Italy

Abstract

Brain decoding is a popular multivariate approach for hypothesis testing in neuroimaging. Linear classifiers are widely employed in the brain decoding paradigm to discriminate among experimental conditions. Then, the derived linear weights are visualized in the form of multivariate brain maps to further study the spatio-temporal patterns of underlying neural activities. It is well known that the brain maps derived from weights of linear classifiers are hard to interpret because of high correlations between predictors, low signal to noise ratios, and the high dimensionality of neuroimaging data. Therefore, improving the interpretability of brain decoding approaches is of primary interest in many neuroimaging studies. Despite extensive studies of this type, at present, there is no formal definition for interpretability of multivariate brain maps. As a consequence, there is no quantitative measure for evaluating the interpretability of different brain decoding methods. In this paper, first, we present a theoretical definition of interpretability in brain decoding; we show that the interpretability of multivariate brain maps can be decomposed into their reproducibility and representativeness. Second, as an application of the proposed definition, we formalize a heuristic method for approximating the interpretability of multivariate brain maps in a binary magnetoencephalography (MEG) decoding scenario. Third, we pro-

*Corresponding author:

Email address: seyedmostafa.kia@unitn.it (Seyed Mostafa Kia)

¹University of Trento, Trento, Italy

²Fondazione Bruno Kessler (FBK), Trento, Italy

³Centro Interdipartimentale Mente e Cervello (CIMeC), Trento, Italy

pose to combine the approximated interpretability and the performance of the brain decoding into a new multi-objective criterion for model selection. Our results for the MEG data show that optimizing the hyper-parameters of the regularized linear classifier based on the proposed criterion results in more informative multivariate brain maps. More importantly, the presented definition provides the theoretical background for quantitative evaluation of interpretability, and hence, facilitates the development of more effective brain decoding algorithms in the future.

Keywords: MVPA, brain decoding, brain mapping, interpretation, model selection

1. Introduction

2 Understanding the mechanisms of the brain has been a crucial topic
3 throughout the history of science. Ancient Greek philosophers envisaged
4 different functionalities for the brain ranging from cooling the body to acting
5 as the seat of the rational soul and the center of sensation [1]. Modern
6 cognitive science, emerging in the 20th century, provides better insight into
7 the brain's functionality. In cognitive science, researchers usually analyze
8 recorded brain activity and behavioral parameters to discover the answers of
9 *where, when, and how* a brain region participates in a particular cognitive
10 process.

11 To answer the key questions in cognitive science, scientists often employ
12 mass-univariate hypothesis testing methods to test scientific hypotheses on a
13 large set of independent variables [2, 3]. Mass-univariate hypothesis testing
14 is based on performing multiple tests, e.g., t-tests, one for each unit of the
15 neuroimaging data, i.e., independent variables. The high spatial and tempo-
16 ral granularity of the univariate tests provides fair level of interpretability.
17 On the down side, the high dimensionality of neuroimaging data requires
18 a large number of tests that reduces the sensitivity of these methods af-
19 ter multiple comparison correction. Although some techniques such as the
20 non-parametric cluster-based permutation test [4, 5] offer more sensitivity
21 because of the cluster assumption, they still experience low sensitivity to
22 brain activities that are narrowly distributed in time and space [2, 6]. The
23 multivariate counterparts of mass-univariate analysis, known generally as
24 multivariate pattern analysis (MVPA), have the potential to overcome these
25 deficits. Multivariate approaches are capable of identifying complex spatio-

26 temporal interactions between different brain areas with higher sensitivity
27 and specificity than univariate analysis [7], especially in group analysis of
28 neuroimaging data [8].

29 *Brain decoding* [9] is an MVPA technique that delivers a model to predict
30 the mental state of a human subject based on the recorded brain signal.
31 There are two potential applications for brain decoding: 1) brain-computer
32 interfaces (BCIs) [10, 11], and 2) multivariate hypothesis testing [12]. In the
33 first case, a brain decoder with maximum prediction power is desired. In the
34 second case, in addition to the prediction power, extra information on the
35 spatio-temporal nature of a cognitive process is desired. In this study, we are
36 interested in the second application of brain decoding that can be considered
37 a multivariate alternative for mass-univariate hypothesis testing.

38 In brain decoding, generally, linear classifiers are used to assess the relation
39 between independent variables, i.e., features, and dependent variables,
40 i.e., cognitive tasks [13, 14, 15]. This assessment is performed by solving a
41 linear optimization problem that assigns weights to each independent variable.
42 Currently, brain decoding is the gold standard in multivariate analysis
43 for functional magnetic resonance imaging (fMRI) [16, 17, 18, 19] and magnetoencephalogram/electroencephalogram (MEEG) studies [20, 21, 22, 23, 24,
44 25, 26]. It has been shown that brain decoding can be used in combination
45 with brain encoding [27] to infer the causal relationship between stimuli and
46 responses [28].

47 *Brain mapping* [29] is a higher form of neuroimaging that assigns pre-
48 computed quantities, e.g., univariate statistics or weights of a linear classifier,
49 to the spatio-temporal representation of neuroimaging data. In MVPA,
50 brain mapping uses the learned parameters from brain decoding to produce
51 brain maps, in which the engagement of different brain areas in a cognitive
52 task is visualized. Intuitively, the interpretability of a brain decoder refers to
53 the level of information that can be reliably derived by an expert from the
54 resulting maps. From the neuroscientific perspective, a brain map is consid-
55 ered *interpretable* if it enables the scientist to answer *where*, *when*, and *how*
56 questions.

57 Typically, a trained classifier is a black box that predicts the label of
58 an unseen data point with some accuracy. Valverde-Albacete and Peláez-
59 Moreno [30] experimentally showed that in a classification task optimizing
60 only classification error rate is insufficient to capture the transfer of crucial
61 information from the input to the output of a classifier. It is also shown
62 by Ramdas et al. [31] that in the case of data with small sample size using

64 the classification accuracy as a test statistic for two sample testing should be
65 performed with extra cautious. Beside these limitations of classification ac-
66 curacy in inference, and considering the fact that the best predictive model
67 might not be the most informative one [32]; a classifier, taken alone, only
68 answers the question of *what* is the most likely label of a given unseen sam-
69 ple [33]. This fact is generally known as knowledge extraction gap [34] in
70 the classification context. Thus far, many efforts have been devoted to filling
71 the knowledge extraction gap of linear and non-linear data modeling meth-
72 ods in different areas such as computer vision [35], signal processing [36],
73 chemometrics [37], bioinformatics [38], and neuroinformatics [39].

74 Despite the theoretical advantages of MVPA, its practical application to
75 inferences regarding neuroimaging data is limited primarily by a lack of in-
76 terpretability [40, 41, 42]. Therefore, improving the interpretability of linear
77 brain decoding and associated brain maps is a primary goal in the brain imag-
78 ing literature [43]. The lack of interpretability of multivariate brain maps is
79 a direct consequence of low signal-to-noise ratios (SNRs), high dimensional-
80 ity of whole-scalp recordings, high correlations among different dimensions of
81 data, and cross-subject variability [15, 44, 45, 14, 46, 47, 48, 49, 50, 51, 52, 41].
82 At present, two main approaches are proposed to enhance the interpretabil-
83 ity of multivariate brain maps: 1) introducing new metrics into the model
84 selection procedure and 2) introducing new penalty terms for regularization
85 to enhance stability selection.

86 The first approach to improving the interpretability of brain decoding
87 concentrates on the model selection procedure. Model selection is a pro-
88 cedure in which the best values for the hyper-parameters of a model are
89 determined [14]. The selection process is generally performed by considering
90 the generalization performance, i.e., the accuracy, of a model as the decisive
91 criterion. Rasmussen et al. [53] showed that there is a trade-off between
92 the spatial reproducibility and the prediction accuracy of a classifier; there-
93 fore, the reliability of maps cannot be assessed merely by focusing on their
94 prediction accuracy. To utilize this finding, they incorporated the spatial re-
95 producibility of brain maps in the model selection procedure. An analogous
96 approach, using a different definition of spatial reproducibility, is proposed
97 by Conroy et al. [54]. Beside spatial reproducibility, the stability of the clas-
98 sifiers [55] is another criterion that is used in combination with generalization
99 performance to enhance the interpretability. For example, [56, 57] showed
100 that incorporating the stability of models into cross-validation improves the
101 interpretability of the estimated parameters (by linear models).

102 The second approach to improving the interpretability of brain decoding
103 focuses on the underlying mechanism of regularization. The main idea be-
104 hind this approach is two-fold: 1) customizing the regularization terms to
105 address the ill-posed nature of brain decoding problems (where the number
106 of samples is much less than the number of features) [58, 50] and 2) combin-
107 ing the structural and functional prior knowledge with the decoding process
108 so as to enhance stability selection. Group Lasso [59] and total-variation
109 penalty [60] are two effective methods using this technique [61, 62]. Sparse
110 penalized discriminant analysis [63], group-wise regularization [7], random-
111 ized Lasso [47], smoothed-sparse logistic regression [64], total-variation L1
112 penalization [65, 66], the graph-constrained elastic-net [67, 68], and random-
113 ized structural sparsity [69] are examples of brain decoding methods in which
114 regularization techniques are employed to improve stability selection, and
115 thus, the interpretability of brain decoding.

116 Recently, taking a new approach to the problem, Haufe et al. questioned
117 the interpretability of weights of linear classifiers because of the contribu-
118 tion of noise in the decoding process [70, 39, 71]. To address this problem,
119 they proposed a procedure to convert the linear brain decoding models into
120 their equivalent generative models. Their experiments on the simulated and
121 fMRI/EEG data illustrate that, whereas the direct interpretation of classifier
122 weights may cause severe misunderstanding regarding the actual underlying
123 effect, their proposed transformation effectively provides interpretable maps.
124 Despite the theoretical soundness, the major challenge of estimating the em-
125 pirical covariance matrix of the small sample size neuroimaging data [72]
126 limits the practical application of this method.

127 In spite of the aforementioned efforts to improve the interpretability of
128 brain decoding, there is still no formal definition for the interpretability of
129 brain decoding in the literature. Therefore, the interpretability of different
130 brain decoding methods are evaluated either qualitatively or indirectly (i.e.,
131 by means of an intermediate property). In qualitative evaluation, to show
132 the superiority of one decoding method over the other (or a univariate map),
133 the corresponding brain maps are compared visually in terms of smooth-
134 ness, sparseness, and coherency using already known facts (see, for exam-
135 ple, [47, 73]). In the second approach, important factors in interpretability
136 such as spatio-temporal reproducibility are evaluated to indirectly assess the
137 interpretability of results (see, for example, [46, 53, 54, 74]). Despite partial
138 effectiveness, there is no general consensus regarding the quantification of
139 these intermediate criteria. For example, in the case of spatial reproducibil-

140 ity, different methods such as correlation [53, 74], dice score [46], or parameter
141 variability [39, 54] are used for quantifying the stability of brain maps, each
142 of which considers different aspects of local or global reproducibility.

143 With the aim of filling this gap, our contribution is three-fold: 1) Assuming that the true solution of brain decoding is available, we present a
144 theoretical definition of the interpretability. Furthermore, we show that the
145 interpretability can be decomposed into the reproducibility and the represen-
146 tativeness of brain maps. 2) As a proof of the concept, we propose a practical
147 heuristic based on event-related fields for quantifying the interpretability of
148 brain maps in MEG decoding scenarios. 3) Finally, we propose the com-
149 bination of the interpretability and the performance of the brain decoding
150 as a new Pareto optimal multi-objective criterion for model selection. We
151 experimentally show that incorporating the interpretability into the model
152 selection procedure provides more reproducible, more neurophysiologically
153 plausible, and (as a result) more interpretable maps.

155 **2. Methods**

156 *2.1. Notation and Background*

157 Let $\mathcal{X} \in \mathbb{R}^p$ be a manifold in Euclidean space that represents the in-
158 put space and $\mathcal{Y} \in \mathbb{R}$ be the output space, where $\mathcal{Y} = \Phi^*(\mathcal{X})$. Then, let
159 $S = \{\mathbf{Z} = (\mathbf{X}, \mathbf{Y}) \mid z_1 = (x_1, y_1), \dots, z_n = (x_n, y_n)\}$ be a training set of n
160 independently and identically distributed (iid) samples drawn from the joint
161 distribution of $\mathcal{Z} = \mathcal{X} \times \mathcal{Y}$ based on an unknown Borel probability measure ρ .
162 In the neuroimaging context, \mathbf{X} indicates the trials of brain recording, e.g.,
163 fMRI, MEG, or EEG signals, and \mathbf{Y} represents the experimental conditions
164 or dependent variables. The goal of brain decoding is to find the function
165 $\Phi_S : \mathbf{X} \rightarrow \mathbf{Y}$ as an estimation of the ideal function $\Phi^* : \mathcal{X} \rightarrow \mathcal{Y}$.

166 As is a common assumption in the neuroimaging context, we assume the
167 true solution of a brain decoding problem is among the family of linear func-
168 tions \mathcal{H} ($\Phi^* \in \mathcal{H}$). Therefore, the aim of brain decoding reduces to finding
169 an empirical approximation of Φ_S , indicated by $\hat{\Phi}$, among all $\Phi \in \mathcal{H}$. This
170 approximation can be obtained by estimating the predictive conditional den-
171 sity $\rho(\mathbf{Y} \mid \mathbf{X})$ by training a parametric model $\rho(\mathbf{Y} \mid \mathbf{X}, \Theta)$ (i.e., a likelihood
172 function), where Θ denotes the parameters of the model. Alternatively, Θ
173 can be estimated by solving a risk minimization problem:

$$\hat{\Theta} = \operatorname{argmin}_{\Theta} \mathcal{L}(\Phi(\mathbf{X}), \Phi_S(\mathbf{X}) + \lambda \Omega(\Theta)) \quad (1)$$

174 where $\mathcal{L} : \mathbf{Z} \times \mathbf{Z} \rightarrow \mathbb{R}^+$ is the loss function, $\Omega : \mathbb{R}^p \rightarrow \mathbb{R}^+$ is the reg-
175 ularization term, and λ is a hyper-parameter that controls the amount of
176 regularization. There are various choices for Ω , each of which reduces the
177 hypothesis space \mathcal{H} to $\mathcal{H}' \subset \mathcal{H}$ by enforcing different prior functional or
178 structural constraints on the parameters of the linear decoding model (see,
179 for example, [75, 76, 60, 77]). The amount of regularization λ is generally de-
180 cided using cross-validation or other data perturbation methods in the model
181 selection procedure.

182 In the neuroimaging context, the estimated parameters of a linear de-
183 coding model $\hat{\Theta}$ can be used in the form of a brain map so as to visualize
184 the discriminative neurophysiological effect. Although the magnitude of $\hat{\Theta}$ is
185 affected by the dynamic range of data and the level of regularization, it has
186 no effect on the predictive power and the interpretability of maps. On the
187 other hand, the direction of $\hat{\Theta}$ affects the predictive power and contains in-
188 formation regarding the importance of and relations among predictors. This
189 type of relational information is very useful when interpreting brain maps in
190 which the relation between different spatio-temporal independent variables
191 can be used to describe how different brain regions interact over time for a
192 certain cognitive process. Therefore, we refer to the normalized parameter
193 vector of a linear brain decoder in the unit hyper-sphere as a multivariate
194 brain map (MBM); we denote it by $\vec{\Theta}$ where $\vec{\Theta} = \frac{\Theta}{\|\Theta\|}$ ($\|\cdot\|$ represents the
195 2-norm of a vector).

196 As shown in Eq. 1, learning occurs using the sampled data. In other
197 words, in the learning paradigm, we attempt to minimize the loss function
198 with respect to Φ_S (and not Φ^*) [78]. Therefore, all of the implicit assump-
199 tions (such as linearity) regarding Φ^* might not hold on Φ_S , and vice versa
200 (see the supplementary material for a simple illustrative example). The *ir-
201 reducible error* ε is the direct consequence of sampling; it sets a lower bound
202 on the error, where we have:

$$\Phi_S(\mathbf{X}) = \Phi^*(\mathbf{X}) + \varepsilon \quad (2)$$

203 The distribution of ε dictates the type of loss function \mathcal{L} in Eq. 1. For
204 example, assuming a Gaussian distribution with mean 0 and variance σ^2 for
205 ε implies the least squares loss function [79].

206 2.2. Interpretability of Multivariate Brain Maps: Theoretical Definition

207 In this section, we present a theoretical definition for the interpretability
208 of linear brain decoding models and their associated MBMs. Our definition

209 of interpretability is based on two main assumptions: 1) the brain decoding
 210 problem is linearly separable; 2) its *unique* and neurophysiologically *plausible*¹
 211 solution, i.e., Φ^* , is available.

212 Consider a linearly separable brain decoding problem in an ideal scenario
 213 where $\varepsilon = 0$ and $rank(\mathbf{X}) = p$. In this case, Φ^* is linear and its parameters Θ^*
 214 are unique and plausible. The unique parameter vector Θ^* can be computed
 215 as follows:

$$\Theta^* = \Sigma_{\mathbf{X}}^{-1} \mathbf{X}^T \mathbf{Y} \quad (3)$$

216 Using Θ^* as the reference, we define the *strong-interpretability* of an MBM
 217 as follows:

218 **Definition 1.** An MBM $\vec{\Theta}$ associated with a linear function Φ is “strongly-
 219 interpretable” if and only if $\vec{\Theta} \propto \Theta^*$.

220 It can be shown that, in practice, the estimated solution of a linear brain
 221 problem (using Eq. 1) is not strongly-interpretable because of the inherent
 222 limitations of neuroimaging data, such as uncertainty [80] in the input and
 223 output space ($\varepsilon \neq 0$), the high dimensionality of data ($n \ll p$), and the
 224 high correlation between predictors ($rank(\mathbf{X}) < p$). With these limitations
 225 in mind, even though in practice the solution of linear brain decoding is not
 226 strongly-interpretable, one can argue that some are more interpretable than
 227 others. For example, in the case in which $\Theta^* \propto [0, 1]^T$, a linear classifier
 228 where $\hat{\Theta} \propto [0.1, 1.2]^T$ can be considered more interpretable than a linear
 229 classifier where $\hat{\Theta} \propto [2, 1]^T$. This issue raises the following question:

230 **Problem 1.** Let S^1, \dots, S^m be m perturbed training sets drawn from S via
 231 a certain perturbation scheme such as jackknife, bootstrapping [81], or cross-
 232 validation [82]. Assume $\vec{\Theta}^1, \dots, \vec{\Theta}^m$ are m MBMs of a certain Φ (estimated
 233 using Eq. 1 for certain \mathcal{L} , Ω , and λ) on the corresponding perturbed training
 234 sets. How can we quantify the proximity of Φ to the strongly-intrepretable
 235 solution of brain decoding problem Φ^* ?

¹Here, neurophysiological plausibility refers to the spatio-temporal chemo-physical constraints of the underlying neural activity that is highly dependent on the acquisition device.

236 To answer this question, considering the uniqueness and the plausibility
237 of Φ^* as the two main characteristics that convey its strong-interpretability,
238 we define the interpretability as follows:

239 **Definition 2.** Let α^j ($j = 1, \dots, m$) be the angle between $\vec{\Theta}^j$ and $\vec{\Theta}^*$. The
240 “interpretability” ($0 \leq \eta_\Phi \leq 1$) of the MBM derived from a linear function
241 Φ is defined as follows:

$$\forall j \in \{1, \dots, m\}, \eta_\Phi = \mathbb{E}_S[\cos(\alpha^j)] \quad (4)$$

242 Empirically, the interpretability is the mean of cosine similarities between
243 Θ^* and MBMs derived from different samplings of the training set. In ad-
244 dition to the fact that employing cosine similarity is a common method for
245 measuring the similarity between vectors, we have another strong motivation
246 for this choice. It can be shown that, for large values of p , the distribution of
247 the dot product in the unit hyper-sphere, i.e., the cosine similarity, converges
248 to a normal distribution with 0 mean and variance of $\frac{1}{p}$, i.e., $\mathcal{N}(0, \sqrt{\frac{1}{p}})$. Due
249 to the small variance for a large enough p values, any similarity value that is
250 significantly larger than zero represents a meaningful similarity between two
251 high dimensional vectors (see the supplementary material for more details
252 about the distribution of cosine similarity).

253 In what follows, we demonstrate how the definition of interpretability is
254 geometrically related to the uniqueness and plausibility characteristics of the
255 true solution to brain decoding problem.

256 *2.3. Interpretability Decomposition into Reproducibility and Representativeness*

257 An alternative approach toward quantifying the interpretability is to as-
258 sess separately its uniqueness and neurophysiological plausibility. In this
259 section, we firstly define the reproducibility and representativeness as mea-
260 sures for quantifying the uniqueness and neurophysiological plausibility of
261 brain decoding model, respectively. Then we show how these definitions are
262 related to the definition of interpretability.

263 The high dimensionality and the high correlations between variables are
264 two inherent characteristics of neuroimaging data that negatively affect the
265 uniqueness of the solution of a brain decoding problem. Therefore, a certain
266 configuration of hyper-parameters may result different estimated parameters

268 on different portions of data. Here, we are interested in assessing this vari-
 269 ability as a measure for uniqueness. Let θ_i^j be the i th ($i = 1, \dots, p$) element
 270 of an MBM estimated on the j th ($j = 1, \dots, m$) perturbed training set. We
 271 first define the *main multivariate brain map* as follows:

272 **Definition 3.** The “main multivariate brain map” $\vec{\Theta}^\mu \in \mathbb{R}^p$ of a linear func-
 273 tion Φ is defined as the sum of estimated MBMs $\vec{\Theta}^j$ ($j = 1, \dots, m$) on the
 274 perturbed training sets S^j in the unit hyper-sphere:

$$\vec{\Theta}^\mu = \frac{\left[\sum_{j=1}^m \theta_1^j \quad \sum_{j=1}^m \theta_2^j \quad \dots \quad \sum_{j=1}^m \theta_p^j \right]^T}{\left\| \left[\sum_{j=1}^m \theta_1^j \quad \sum_{j=1}^m \theta_2^j \quad \dots \quad \sum_{j=1}^m \theta_p^j \right]^T \right\|} \quad (5)$$

275 The definition of $\vec{\Theta}^\mu$ is analogous to the main prediction of a learning
 276 algorithm [83]; it provides a reference for quantifying the reproducibility of
 277 an MBM:

278 **Definition 4.** Let $\vec{\Theta}^\mu$ be the main multivariate brain map of Φ . Then, let
 279 α^j be the angle between $\vec{\Theta}^j$ and $\vec{\Theta}^\mu$. The “reproducibility” ψ_Φ ($0 \leq \psi_\Phi \leq 1$)
 280 of an MBM derived from a linear function Φ is defined as follows:

$$\forall j \in \{1, \dots, m\}, \psi_\Phi = \mathbb{E}_S[\cos(\alpha^j)] \quad (6)$$

281 In fact, reproducibility provides a measure for quantifying the dispersion
 282 of MBMs, computed over different perturbed training sets, from the main
 283 multivariate brain map.

284 On the other hand, the coherency between the main multivariate brain
 285 map of a decoder and the true solution can be employed as a measure for the
 286 plausibility of a model. We refer to this coherency as the *representativeness*
 287 of an MBM:

288 **Definition 5.** Let $\vec{\Theta}^\mu$ be the main multivariate brain map of Φ . The “rep-
 289 resentativeness” ($0 \leq \beta_\Phi \leq 1$) is defined as the cosine similarity between $\vec{\Theta}^\mu$
 290 and $\vec{\Theta}^*$:

$$\beta_\Phi = \frac{|\vec{\Theta}^\mu \cdot \vec{\Theta}^*|}{\|\vec{\Theta}^\mu\| \|\vec{\Theta}^*\|} \quad (7)$$

291 The following proposition shows the relationship between the presented
292 definitions for reproducibility, representativeness, and the interpretability:

293 **Proposition 1.** $\eta_\Phi = \beta_\Phi \times \psi_\Phi$.

294 See Appendix D for a proof. Proposition 1 indicates the interpretability
295 can be decomposed into the representativeness and the reproducibility of a
296 decoding model.

297 *2.4. A Heuristic for Practical Quantification of Interpretability in Time-
298 Domain MEG decoding*

299 In practice, it is impossible to evaluate the interpretability, as Φ^* is un-
300 known. In this study, to provide a practical proof of the mentioned theoret-
301 ical concepts, we propose the use of contrast event-related fields (cERFs) of
302 MEG data as neurophysiological plausible heuristics for Θ^* in a binary MEG
303 decoding scenario in the time domain.

304 The EEG/MEG data are a mixture of several simultaneous stimulus-
305 related and stimulus-unrelated brain activities. In general, unrelated-stimulus
306 brain activities are considered as Gaussian noise with zero mean and variance
307 σ^2 . One popular approach to canceling the noise component is to compute
308 the average of multiple trials. It is expected that the average will converge
309 to the true value of the signal with a variance of $\frac{\sigma^2}{n}$. The result of the av-
310 eraging process is generally known as ERF in the MEG context; separate
311 interpretation of different ERF components can be performed [84]¹.

312 Assume $\mathbf{X}^+ = \{x_i \in \mathbf{X} \mid y_i = 1\} \in \mathbb{R}^{n^+ \times p}$ and $\mathbf{X}^- = \{x_i \in \mathbf{X} \mid y_i =$
313 $-1\} \in \mathbb{R}^{n^- \times p}$. Then, the cERF brain map $\vec{\Theta}^{cERF}$ is computed as follows:

$$\vec{\Theta}^{cERF} = \frac{\frac{1}{n^+} \sum_{x_i \in X^+} x_i - \frac{1}{n^-} \sum_{x_i \in X^-} x_i}{\left\| \frac{1}{n^+} \sum_{x_i \in X^+} x_i - \frac{1}{n^-} \sum_{x_i \in X^-} x_i \right\|} \quad (8)$$

314 Using the core theory presented in [39], it can be shown that cERF is
315 the equivalent generative model for the least squares solution in a binary

¹The application of the presented heuristic to MEG data can be extended to EEG because of the inherent similarity of the measured neural correlates in these two devices. In the EEG context, the ERF can be replaced by the event-related potential (ERP).

316 time-domain MEG decoding scenario (see Appendix A). Using $\vec{\Theta}^{cERF}$ as a
 317 heuristic for $\vec{\Theta}^*$, the representativeness can be approximated as follows:

$$\tilde{\beta}_\Phi = \frac{|\vec{\Theta}^\mu \cdot \vec{\Theta}^{cERF}|}{\|\vec{\Theta}^\mu\| \|\vec{\Theta}^{cERF}\|} \quad (9)$$

318 Where $\tilde{\beta}_\Phi$ is an approximation of β_Φ and we have:

$$\beta_\Phi = \Delta_\beta \tilde{\beta}_\Phi \pm \sqrt{(1 - \tilde{\beta}_\Phi^2)(1 - \Delta_\beta^2)} \quad (10)$$

319 Δ_β represents the cosine similarity between $\vec{\Theta}^*$ and $\vec{\Theta}^{cERF}$ (see Fig-
 320 ures B.8 and Appendix B). If $\Delta_\beta \rightarrow 1$ then $\tilde{\beta}_\Phi \rightarrow \beta_\Phi$.

321 In a similar manner, $\vec{\Theta}^{cERF}$ can be used to heuristically approximate the
 322 interpretability as follows:

$$\tilde{\eta}_\Phi = \forall j \in \{1, \dots, m\}, \tilde{\eta}_\Phi = \mathbb{E}_S(\cos(\gamma^j)) \quad (11)$$

323 where $\gamma_1, \dots, \gamma_m$ are the angles between $\vec{\Theta}^1, \dots, \vec{\Theta}^m$ and $\vec{\Theta}^{cERF}$. The
 324 following equality represents the relation between η and $\tilde{\eta}$ (see Figures C.9
 325 and Appendix C).

$$\eta_\Phi = \Delta_\beta \tilde{\eta}_\Phi \pm \sqrt{1 - \Delta_\beta^2} \frac{1}{m} (\sin \gamma_1 + \dots + \sin \gamma_m) \quad (12)$$

326 Again, if $\Delta_\beta \rightarrow 1$ then $\tilde{\eta}_\Phi \rightarrow \eta_\Phi$. Notice that Δ_β is independent of the
 327 decoding approach used; it only depends on the quality of the heuristic. It
 328 can be shown that $\tilde{\eta}_\Phi = \tilde{\beta}_\Phi \times \psi_\Phi$.

329 Eq. 12 shows that the choice of heuristic has a direct effect on the approxi-
 330 mation of interpretability and that an inappropriate selection of the heuristic
 331 yields a very poor estimation of interpretability because of the destructive
 332 contribution of Δ_β . Therefore, the choice of heuristic should be carefully
 333 justified based on accepted and well-defined facts regarding the nature of the
 334 collected data (see the supplementary material for the experimental investi-
 335 gation of the limitations of the proposed heuristic).

336 *2.5. Incorporating the Interpretability into Model Selection*

337 The procedure for evaluating the performance of a model so as to choose
 338 the best values for hyper-parameters is known as *model selection* [85]. This
 339 procedure generally involves numerical optimization of the model selection
 340 criterion. The most common model selection criterion is based on an estima-
 341 tor of generalization performance, i.e., the predictive power. In the context
 342 of brain decoding, especially when the interpretability of brain maps matters,
 343 employing the predictive power as the only decisive criterion in model selec-
 344 tion is problematic in terms of interpretability [86, 53, 54]. Here, we propose
 345 a multi-objective criterion for model selection that takes into account both
 346 prediction accuracy and MBM interpretability.

347 Let $\tilde{\eta}_\Phi$ and δ_Φ be the approximated interpretability and the generalization
 348 performance of a linear function Φ , respectively. We propose the use of the
 349 *scalarization* technique [87] for combining $\tilde{\eta}_\Phi$ and δ_Φ into one scalar $0 \leq$
 350 $\zeta(\Phi) \leq 1$ as follows:

$$\zeta_\Phi = \begin{cases} \frac{\omega_1 \tilde{\eta}_\Phi + \omega_2 \delta_\Phi}{\omega_1 + \omega_2} & \delta_\Phi \geq \kappa \\ 0 & \delta_\Phi < \kappa \end{cases} \quad (13)$$

351 where ω_1 and ω_2 are weights that specify the level of importance of the
 352 interpretability and the performance, respectively. κ is a threshold on the
 353 performance that filters out solutions with poor performance. In classification
 354 scenarios, κ can be set by adding a small safe interval to the chance level of
 355 classification.

356 It can be shown that the hyper-parameters of a model Φ are optimized
 357 based on ζ_Φ are Pareto optimal [88]. In other words, there exist no other Φ'
 358 for which we obtain both $\tilde{\eta}_{\Phi'} > \tilde{\eta}_\Phi$ and $\delta_{\Phi'} > \delta_\Phi$. We expect that optimizing
 359 the hyper-parameters based on ζ_Φ , rather only δ_Φ , yields more informative
 360 MBMs.

361 *2.6. Experimental Materials*

362 *2.6.1. Toy Dataset*

363 To illustrate the importance of integrating the interpretability of brain
 364 decoding with the model selection procedure, we use simple 2-dimensional toy
 365 data presented in [39]. Assume that the true underlying generative function
 366 Φ^* is defined by

$$\mathcal{Y} = \Phi^*(\mathcal{X}) = \begin{cases} 1 & \text{if } x_1 = 1.5 \\ -1 & \text{if } x_1 = -1.5 \end{cases}$$

367 where $\mathcal{X} \in \{[1.5, 0]^T, [-1.5, 0]^T\}$; and x_1 and x_2 represent the first and
368 the second dimension of the data, respectively. Furthermore, assume the
369 data is contaminated by Gaussian noise with co-variance $\Sigma = \begin{bmatrix} 1.02 & -0.3 \\ -0.3 & 0.15 \end{bmatrix}$.

370 Figure 1 shows the distribution of the noisy data.

371 2.6.2. MEG Data

372 We use the MEG dataset presented in [89]¹. The dataset was also used
373 for the DecMeg2014 competition². In this dataset, visual stimuli consisting
374 of famous faces, unfamiliar faces, and scrambled faces are presented to 16
375 subjects and fMRI, EEG, and MEG signals are recorded. Here, we are only
376 interested in MEG recordings. The MEG data were recorded using a Vec-
377 torView system (Elekta Neuromag, Helsinki, Finland) with a magnetometer
378 and two orthogonal planar gradiometers located at 102 positions in a hemi-
379 spherical array in a light Elekta-Neuromag magnetically shielded room.

380 Three major reasons motivated the choice of this dataset: 1) It is publicly
381 available. 2) The spatio-temporal dynamic of the MEG signal for face vs.
382 scramble stimuli has been well studied. The event-related potential analysis
383 of EEG/MEG shows that $N170$ occurs $130 - 200ms$ after stimulus presen-
384 tation and reflects the neural processing of faces [90, 89]. Therefore, the
385 $N170$ component can be considered the ground truth for our analysis. 3) In
386 the literature, non-parametric mass-univariate analysis such as cluster-based
387 permutation tests is unable to identify narrowly distributed effects in space
388 and time (e.g., an $N170$ component) [2, 6]. These facts motivate us to employ
389 multivariate approaches that are more sensitive to these effects.

390 As in [51], we created a balanced face vs. scrambled MEG dataset by
391 randomly drawing from the trials of unscrambled (famous or unfamiliar) faces
392 and scrambled faces in equal number. The samples in the face and scrambled
393 face categories are labeled as 1 and -1 , respectively. The raw data is high-
394 pass filtered at $1Hz$, down-sampled to $250Hz$, and trimmed from $200ms$
395 before the stimulus onset to $800ms$ after the stimulus. Thus, each trial has
396 250 time-points for each of the 306 MEG sensors (102 magnetometers and

¹The full dataset is publicly available at ftp://ftp.mrc-cbu.cam.ac.uk/personal/rik.henson/wakemandg_hensonrn/

²The competition data are available at <http://www.kaggle.com/c/decoding-the-human-brain>

397 204 planar gradiometers)¹. To create the feature vector of each sample, we
398 pooled all of the temporal data of 306 MEG sensors into one vector (i.e.,
399 we have $p = 250 \times 306 = 76500$ features for each sample). Before training
400 the classifier, all of the features are standardized to have a mean of 0 and
401 standard-deviation of 1.

402 *2.7. Classification and Evaluation*

403 In all experiments, a least squares classifier with L1-penalization, i.e.,
404 Lasso [75], is used for decoding. Lasso is a very popular classification method
405 in the context of brain decoding, mainly because of its sparsity assumption.
406 The choice of Lasso helps us to better illustrate the importance of includ-
407 ing the interpretability in the model selection. Lasso solves the following
408 optimization problem:

$$\hat{\Theta} = \operatorname{argmin}_{\Theta} \|\Phi(\mathbf{X}) - \Phi_S(\mathbf{X})\|_2^2 + \lambda \|\Theta\|_1 \quad (14)$$

409 where λ is the hyper-parameter that specifies the level of regularization.
410 Therefore, the aim of the model selection is to find the best value for λ .
411 Here, we try to find the best regularization parameter value among $\lambda =$
412 $\{0.001, 0.01, 0.1, 1, 10, 50, 100, 250, 500, 1000, 5000, 10000, 15000, 25000, 50000\}$.

413 We use the out-of-bag (OOB) [91, 92] method for computing δ_{Φ} , ψ_{Φ} , $\tilde{\beta}_{\Phi}$,
414 $\tilde{\eta}_{\Phi}$, and ζ_{Φ} for different values of λ . In OOB, given a training set (\mathbf{X}, \mathbf{Y}) ,
415 m replications of bootstrap [81] are used to create perturbed training sets
416 (we set $m = 50$)². In all of our experiments, we set $\omega_1 = \omega_2 = 1$ and
417 $\kappa = 0.6$ in the computation of ζ_{Φ} . Furthermore, we set $\delta_{\Phi} = 1 - EPE$
418 where EPE indicates the expected prediction error; it is computed using the
419 procedure explained in Appendix E. Employing OOB provides the possibility
420 of computing the bias and variance of the model as contributing factors in
421 EPE.

422 To investigate the behavior of the proposed model selection criterion,
423 we benchmark it against the commonly used performance criterion in the
424 single-subject decoding scenario. Assuming $(\mathbf{X}_i, \mathbf{Y}_i)$ for $i = 1, \dots, 16$ are
425 MEG trial/label pairs for subject i , we separately train a Lasso model for

¹The preprocessing scripts in python and MATLAB are available at: <https://github.com/FBK-NILab/DecMeg2014/>

²The MATLAB code used for experiments is available at <https://github.com/smkia/interpretability/>

426 each subject to estimate the parameter of the linear function $\hat{\Phi}_i$, where $\mathbf{Y}_i =$
427 $\mathbf{X}_i \hat{\Theta}_i$. Let $\hat{\Phi}_i^\delta$ and $\hat{\Phi}_i^\zeta$ represent the optimized solution based on δ_Φ and ζ_Φ ,
428 respectively. We denote the MBM associated with $\hat{\Phi}_i^\delta$ and $\hat{\Phi}_i^\zeta$ by $\vec{\Theta}_i^\delta$ and $\vec{\Theta}_i^\zeta$,
429 respectively. Therefore, for each subject, we compare the resulting decoders
430 and MBMs computed based on these two model selection criteria.

431 **3. Results**

432 *3.1. Performance-Interpretability Dilemma: A Toy Example*

433 In the definition of Φ^* on the toy dataset discussed in Section 2.6.1, x_1 is
434 the decisive variable and x_2 has no effect on the classification of the data into
435 target classes. Therefore, excluding the effect of noise and based on the the-
436 ory of the maximal margin classifier [93, 94], $\vec{\Theta}^* \propto [1, 0]^T$ is the true solution
437 to the decoding problem. By accounting for the effect of noise and solving
438 the decoding problem in (\mathbf{X}, \mathbf{Y}) space, we have $\vec{\Theta} \propto [\frac{1}{\sqrt{5}}, \frac{2}{\sqrt{5}}]^T$ as the
439 parameter of the linear classifier. Although the estimated parameters on the
440 noisy data yield the best generalization performance for the noisy samples,
441 any attempt to interpret this solution fails, as it yields the wrong conclusion
442 with respect to the ground truth (it says x_2 has twice the influence of x_1
443 on the results, whereas it has no effect). This simple experiment shows that
444 the most accurate model is not always the most interpretable one, primarily
445 because the contribution of the noise in the decoding process [39]. On the
446 other hand, the true solution of the problem $\vec{\Theta}^*$ does not provide the best
447 generalization performance for the noisy data.

448 To illustrate the effect of incorporating the interpretability in the model
449 selection, a Lasso model with different λ values is used for classifying the toy
450 data. In this case, because $\vec{\Theta}^*$ is known, the exact value of interpretability can
451 be computed using Eq. 4. Table 1 compares the resultant performance and
452 interpretability from Lasso. Lasso achieves its highest performance ($\delta_\Phi =$
453 0.9884) at $\lambda = 10$ with $\vec{\Theta} \propto [0.4636, 0.8660]^T$ (indicated by the magenta
454 line in Figure 1). Despite having the highest performance, this solution
455 suffers from a lack of interpretability ($\eta_\Phi = 0.4484$). By increasing λ , the
456 interpretability improves so that for $\lambda = 500, 1000$ the classifier reaches its
457 highest interpretability by compensating for 0.06 of its performance. Our
458 observation highlights two main points:

459 1. In the case of noisy data, the interpretability of a decoding model is
460 incoherent with its performance. Thus, optimizing the parameter of

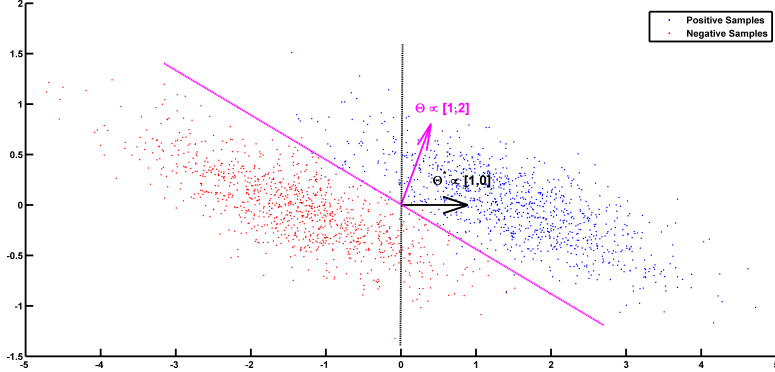


Figure 1: Noisy samples of toy data. The black line shows the true separator based on the generative model (Φ^*). The magenta line shows the most accurate classification solution. Because of the contribution of noise, any interpretation of the parameters of the most accurate classifier yields a misleading conclusion with respect to the true underlying phenomenon [39].

Table 1: Comparison between δ_Φ , η_Φ , and ζ_Φ for different λ values on the toy 2D example shows the performance-interpretability dilemma, in which the most accurate classifier is not the most interpretable one.

λ	0	0.001	0.01	0.1	1	10	50	100	250	500	1000
$\delta(\Phi)$	0.9883	0.9883	0.9883	0.9883	0.9883	0.9884	0.9880	0.9840	0.9310	0.9292	0.9292
$\eta(\Phi)$	0.4391	0.4391	0.4391	0.4392	0.4400	0.4484	0.4921	0.5845	0.9968	1	1
$\zeta(\Phi)$	0.7137	0.7137	0.7137	0.7137	0.7142	0.7184	0.7400	0.7842	0.9639	0.9646	0.9646
$\tilde{\Theta} \propto$	$\begin{bmatrix} 0.4520 \\ 0.8920 \end{bmatrix}$	$\begin{bmatrix} 0.4520 \\ 0.8920 \end{bmatrix}$	$\begin{bmatrix} 0.4520 \\ 0.8920 \end{bmatrix}$	$\begin{bmatrix} 0.4521 \\ 0.8919 \end{bmatrix}$	$\begin{bmatrix} 0.4532 \\ 0.8914 \end{bmatrix}$	$\begin{bmatrix} 0.4636 \\ 0.8660 \end{bmatrix}$	$\begin{bmatrix} 0.4883 \\ 0.8727 \end{bmatrix}$	$\begin{bmatrix} 0.5800 \\ 0.8146 \end{bmatrix}$	$\begin{bmatrix} 0.99 \\ 0.02 \end{bmatrix}$	$\begin{bmatrix} 1 \\ 0 \end{bmatrix}$	$\begin{bmatrix} 1 \\ 0 \end{bmatrix}$

461 the model based on its performance does not necessarily improve its
462 interpretability. This observation confirms the previous finding by Ras-
463 mussen et al. [53] regarding the trade-off between the spatial repro-
464 ducibility (as a measure for the interpretability) and the prediction
465 accuracy in brain decoding.

466 2. If the right criterion is used in the model selection, employing proper
467 regularization technique (sparsity prior, in this case) leads to more
468 interpretability for the decoding models.

469 *3.2. Mass-Univariate Hypothesis Testing on MEG Data*

470 Results show that non-parametric mass-univariate analysis is unable to
471 detect narrowly distributed effects in space and time (e.g., an *N170* com-
472 ponent) [2, 6]. To illustrate the advantage of the proposed decoding framework

473 for spotting these effects, we performed a non-parametric cluster-based per-
474 mutation test [5] on our MEG dataset using Fieldtrip toolbox [95]. In a single
475 subject analysis scenario, we considered the trials of MEG recordings as the
476 unit of observation in a between-trials experiment. Independent-samples t-
477 statistics are used as the statistics for evaluating the effect at the sample level
478 and to construct spatio-temporal clusters. The maximum of the cluster-level
479 summed t-value is used for the cluster level statistics; the significance prob-
480 ability is computed using a Monte Carlo method. The minimum number
481 of neighboring channels for computing the clusters is set to 2. Considering
482 0.025 as the two-sided threshold for testing the significance level and repeat-
483 ing the procedure separately for magnetometers and combined-gradiometers,
484 no significant result is found for any of the 16 subjects. This result motivates
485 the search for more sensitive (and, at the same time, more interpretable)
486 alternatives for hypothesis testing.

487 *3.3. Single-Subject Decoding on MEG Data*

488 In this experiment, we aim to compare the multivariate brain maps of
489 brain decoding models when δ_Φ and ζ_Φ are used as the criteria for model
490 selection. Figure 2(a) represents the mean and standard-deviation of the
491 performance and interpretability of Lasso across 16 subjects for different
492 λ values. The performance and interpretability curves further illustrate the
493 performance-interpretability dilemma in the single-subject decoding scenario
494 in which increasing the performance delivers less interpretability. The aver-
495 age performance across subjects is improved when λ approaches 1, but on the
496 other side, the reproducibility and the representativeness of models declines
497 significantly [see Figure 2(b)].

498 One possible reason behind the performance-interpretability dilemma is
499 illustrated in Figure 3. The figure shows the mean and standard deviation of
500 bias, variance, and EPE of Lasso across 16 subjects. The plot proposes that
501 the effect of variance is overwhelmed by bias in the computation of EPE,
502 where the best performance (minimum EPE) at $\lambda = 1$ has the lowest bias,
503 its variance is higher than for $\lambda = 0.001, 0.01, 0.1$. While this tiny increase
504 in the variance is not reflected in EPE but Figure 2(b) shows a significant
505 effect on the reproducibility.

506 Table 2 summarizes the performance, reproducibility, representativeness,
507 and interpretability of $\hat{\Phi}_i^\delta$ and $\hat{\Phi}_i^\zeta$ for 16 subjects. The average result over
508 16 subjects shows that employing ζ_Φ instead of δ_Φ in model selection pro-
509 vides significantly higher reproducibility, representativeness, and (as a result)

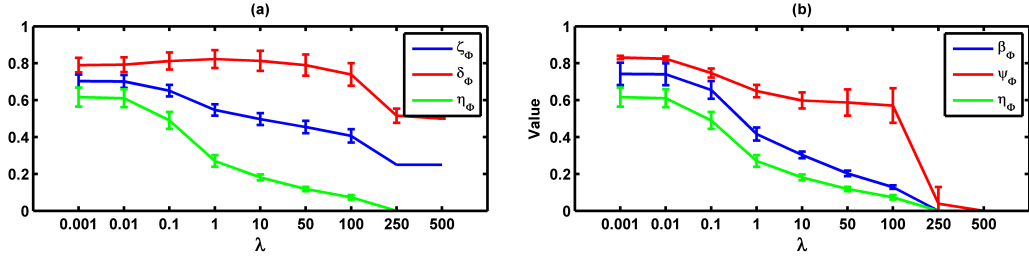


Figure 2: (a) Mean and standard-deviation of the performance, interpretability, and plausibility of Lasso over 16 subjects. The performance and interpretability become incoherent as λ increases. (b) Mean and standard-deviation of the reproducibility, representativeness, and interpretability of Lasso over 16 subjects. The interpretability declines because of the decrease in both reproducibility and representativeness.

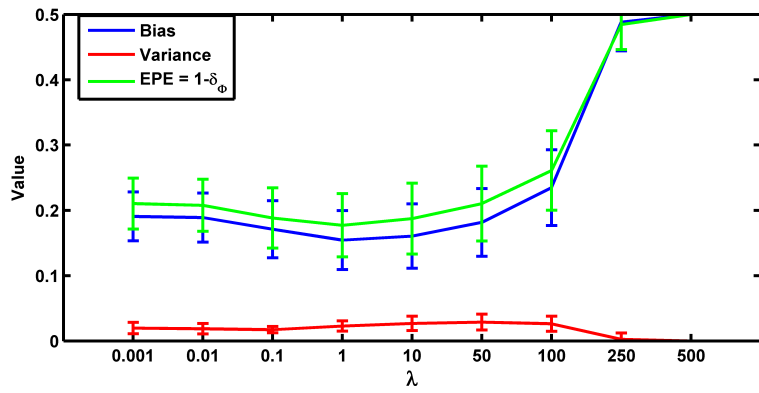


Figure 3: Mean and standard-deviation of the bias, variance, and EPE of Lasso over 16 subjects. The effect of variance on the EPE is overwhelmed by bias.

Table 2: The performance, reproducibility, representativeness, and interpretability of $\hat{\Phi}_i^\delta$ and $\hat{\Phi}_i^\zeta$ over 16 subjects.

Subj	Criterion: δ_Φ					Criterion: ζ_Φ				
	δ_Φ	ζ_Φ	$\tilde{\eta}_\Phi$	β_Φ	ψ_Φ	δ_Φ	ζ_Φ	$\tilde{\eta}_\Phi$	β_Φ	ψ_Φ
1	0.81	0.53	0.26	0.42	0.62	0.78	0.70	0.63	0.76	0.83
2	0.80	0.70	0.60	0.72	0.83	0.80	0.70	0.60	0.72	0.83
3	0.81	0.63	0.45	0.64	0.71	0.78	0.71	0.64	0.78	0.83
4	0.84	0.52	0.20	0.31	0.66	0.76	0.70	0.64	0.77	0.83
5	0.80	0.54	0.29	0.44	0.65	0.78	0.69	0.61	0.73	0.83
6	0.79	0.52	0.24	0.39	0.63	0.74	0.67	0.61	0.74	0.82
7	0.84	0.55	0.27	0.40	0.66	0.81	0.70	0.59	0.71	0.84
8	0.87	0.55	0.24	0.35	0.68	0.85	0.68	0.52	0.61	0.84
9	0.80	0.55	0.31	0.46	0.67	0.77	0.67	0.57	0.69	0.82
10	0.79	0.53	0.26	0.41	0.64	0.77	0.68	0.58	0.70	0.83
11	0.74	0.65	0.56	0.68	0.82	0.74	0.65	0.56	0.68	0.82
12	0.80	0.55	0.29	0.46	0.64	0.79	0.70	0.61	0.74	0.83
13	0.83	0.50	0.18	0.29	0.61	0.77	0.70	0.63	0.76	0.82
14	0.90	0.58	0.27	0.39	0.68	0.81	0.78	0.74	0.89	0.84
15	0.92	0.63	0.34	0.48	0.71	0.89	0.78	0.66	0.77	0.86
16	0.87	0.55	0.23	0.37	0.62	0.81	0.74	0.67	0.81	0.83
Mean	0.83±0.05	0.57 ± 0.05	0.31 ± 0.12	0.45 ± 0.13	0.68 ± 0.07	0.79 ± 0.04	0.70±0.04	0.62±0.05	0.74±0.06	0.83±0.01

510 interpretability compensating for 0.04 of performance.

511 These results are further analyzed in Figure 4 where $\hat{\Phi}_i^\delta$ and $\hat{\Phi}_i^\zeta$ are compared subject-wise in terms of their performance and interpretability. The 512 comparison shows that adopting ζ_Φ instead of δ_Φ as the criterion for model 513 selection yields significantly better interpretable models by compensating 514 a negligible degree of performance in 14 out of 16 subjects. Figure 4(a) 515 shows that employing δ_Φ provides on average slightly higher accurate models 516 (Wilcoxon rank sum test p-value= 0.012) across subjects (0.83 ± 0.05) than 517 using ζ_Φ (0.79 ± 0.04). On the other side, Figure 4(b) shows that employing ζ_Φ 518 and compensating by 0.04 in the performance provides (on average) substantially 519 higher (Wilcoxon rank sum test p-value= 5.6×10^{-6}) interpretability 520 across subjects (0.62 ± 0.05) compared to δ_Φ (0.31 ± 0.12). For example, in 521 the case of subject 1 (see table 2), using δ_Φ in model selection to select the 522 best λ value for the Lasso yields a model with $\delta_\Phi = 0.81$ and $\tilde{\eta}_\Phi = 0.26$. In 523 contrast, using ζ_Φ delivers a model with $\delta_\Phi = 0.78$ and $\tilde{\eta}_\Phi = 0.63$. 524

525 The advantage of the exchange between the performance and the interpretability 526 can be seen in the quality of MBMs. Figure 5a and 5b show 527 $\hat{\Theta}_1^\delta$ and $\hat{\Theta}_1^\zeta$ of subject 1, i.e., the spatio-temporal multivariate maps of the 528 Lasso models with maximum values of δ_Φ and ζ_Φ , respectively. The maps 529 are plotted for 102 magnetometer sensors. In each case, the time course of 530 weights of classifiers associated with the MEG2041 and MEG1931 sensors 531 are plotted. Furthermore, the topographic maps represent the spatial pat-

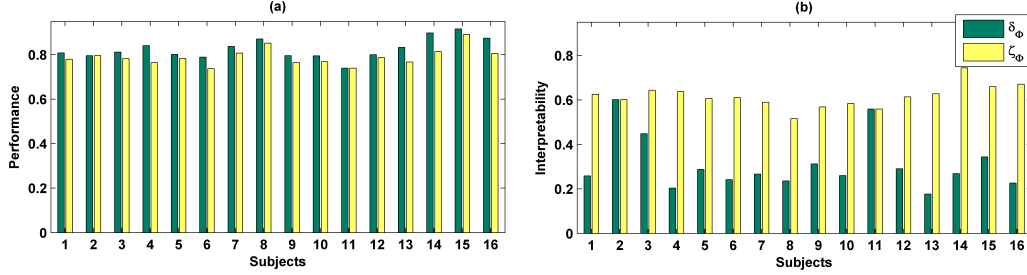
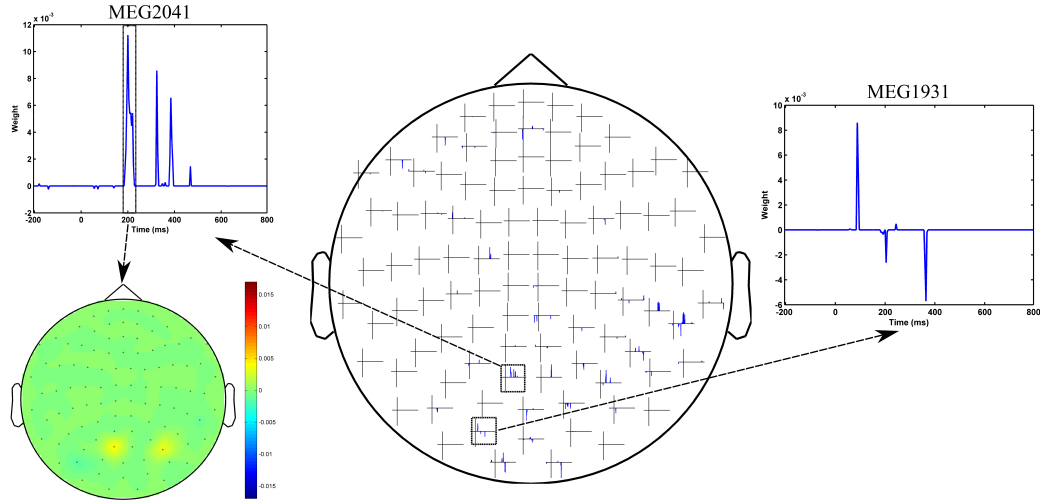


Figure 4: a) Comparison between performance of $\hat{\Phi}_i^\delta$ and $\hat{\Phi}_i^\zeta$. Adopting ζ_Φ instead of δ_Φ in model selection yields (on average) 0.04 less accurate classifiers over 16 subjects. b) Comparison between interpretability of $\hat{\Phi}_i^\delta$ and $\hat{\Phi}_i^\zeta$. Adopting ζ_Φ instead of δ_Φ in model selection yields on average 0.31 more interpretable classifiers over 16 subjects.

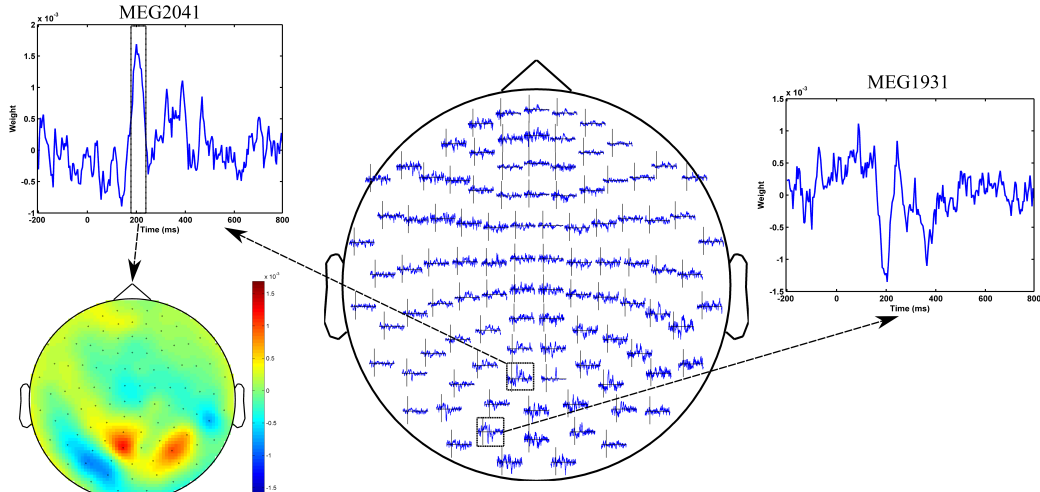
532 terms of weights averaged between 184ms and 236ms after stimulus onset¹.
 533 While $\vec{\Theta}_1^\delta$ is sparse in time and space, it fails to accurately represent the
 534 spatio-temporal dynamic of the N170 component. Furthermore, the multi-
 535 collinearity problem arising from the correlation between the time course of
 536 the MEG2041 and MEG1931 sensors causes extra attenuation of the N170
 537 effect in the MEG1931 sensor. Therefore, the model is unable to capture the
 538 spatial pattern of the dipole in the posterior area. In contrast, $\vec{\Theta}_1^\zeta$ represents
 539 the dynamic of the N170 component in time (see Figure 6). In addition,
 540 it also shows the spatial pattern of two dipoles in the posterior and tem-
 541 poral areas. In summary, $\vec{\Theta}_1^\zeta$ suggests a more representative pattern of the
 542 underlying neurophysiological effect than $\vec{\Theta}_1^\delta$.

543 In addition, optimizing the hyper-parameters of brain decoding based on
 544 ζ_Φ offers more reproducible brain decoders. According to table 2, using ζ_Φ in-
 545 stead of δ_Φ provides (on average) 0.15 more reproducibility over 16 subjects.
 546 To illustrate the advantage of higher reproducibility on the interpretability
 547 of maps, Figure 7 visualizes $\vec{\Theta}_1^\delta$ and $\vec{\Theta}_1^\zeta$ over 4 perturbed training sets. The
 548 spatial maps [Figure 7(a) and Figure 7(c)] are plotted for the magnetometer
 549 sensors averaged in the time interval between 184ms and 236ms after stim-
 550 ulus onset. The temporal maps [Figure 7(b) and Figure 7(d)] are showing

¹The bounds of colorbars are symmetrized based on the maximum absolute value of parameters



(a) Spatio-temporal pattern of $\vec{\Theta}_1^\delta$.



(b) Spatio-temporal pattern of $\vec{\Theta}_1^\zeta$.

Figure 5: Comparison between spatio-temporal multivariate maps of the most accurate (5a) and the most interpretable (5b) classifiers for Subject 1. $\vec{\Theta}_1^\zeta$ provides more spatio-temporal representativeness of the N170 effect than $\vec{\Theta}_1^\delta$.

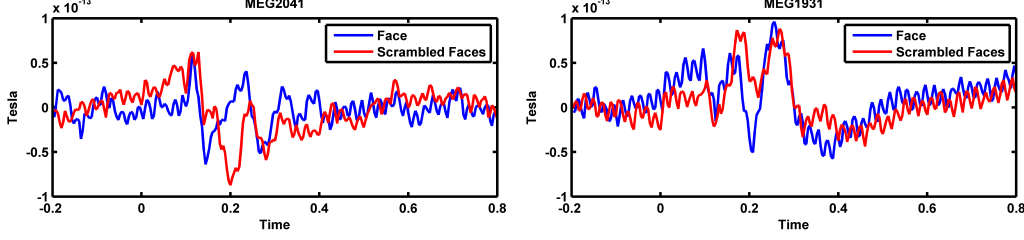


Figure 6: Event related fields (ERFs) of face and scrambled face samples for MEG2041 and MEG1931 sensors.

551 the multivariate temporal maps of MEG1931 and MEG2041 sensors. While
 552 $\vec{\Theta}_1^\delta$ is unstable in time and space across the 4 perturbed training sets, $\vec{\Theta}_1^\zeta$
 553 provides more reproducible maps.

554 **4. Discussions**

555 *4.1. Defining Interpretability: Theoretical Advantages*

556 An overview of the brain decoding literature shows frequent co-occurrence
 557 of the terms interpretation, interpretable, and interpretability with the terms
 558 model, classification, parameter, decoding, method, feature, and pattern (see
 559 the quick meta-analysis on the literature in the supplementary material);
 560 however, a formal formulation of the interpretability is never presented. In
 561 this study, our primary interest is to present a theoretical definition of the
 562 interpretability of linear brain decoding models and their corresponding MBMs.
 563 Furthermore, we show the way in which interpretability is related to the re-
 564 producibility and neurophysiological representativeness of MBMs. Our def-
 565 nition and quantification of interpretability remains theoretical, as we assume
 566 that the true solution of the brain decoding problem is available. Despite
 567 this limitation, we argue that the presented definition provides a concrete
 568 framework of a previously abstract concept and that it establishes a theore-
 569 ical background to explain an ambiguous phenomenon in the brain decoding
 570 context. We support our argument using an example in time-domain MEG
 571 decoding in which we show how the presented definition can be exploited
 572 to heuristically approximate the interpretability. This example shows how

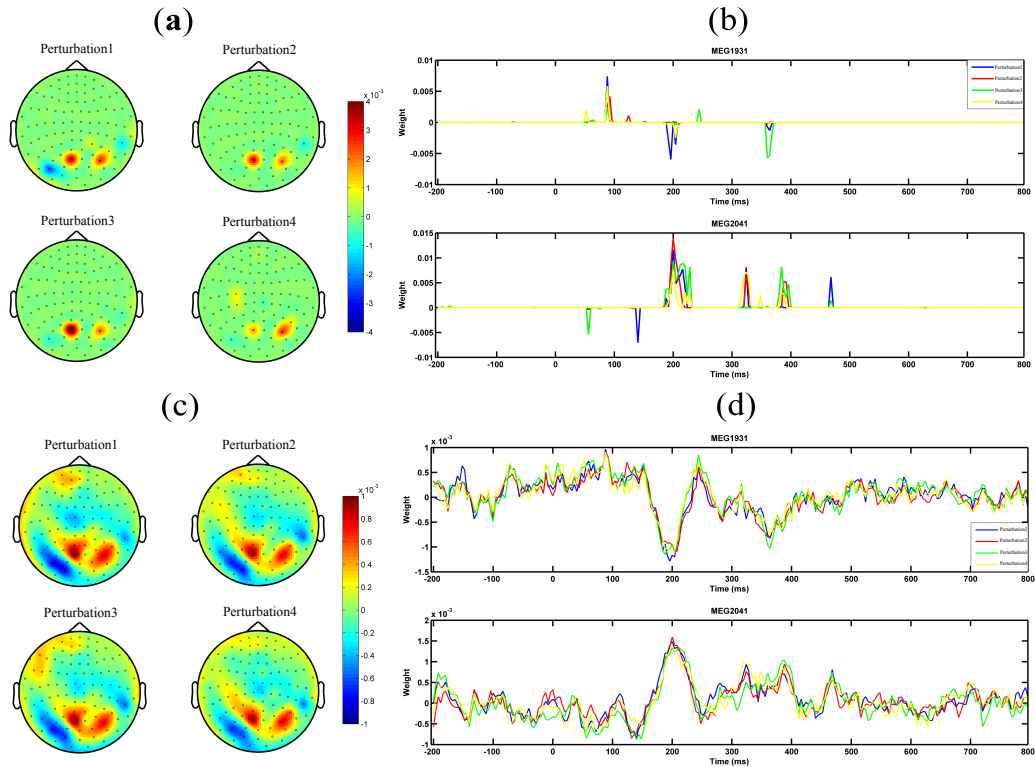


Figure 7: Comparison of the reproducibility of Lasso when δ_Φ and ζ_Φ are used in the model selection procedure. (a) and (b) show the spatio-temporal patterns represented by $\tilde{\Theta}_1^\delta$ across the 4 perturbed training sets. (c) and (d) show the spatio-temporal patterns represented by $\tilde{\Theta}_1^\zeta$ across the 4 perturbed training sets. Employing ζ_Φ instead of δ_Φ in the model selection yields more reproducible MBMs.

573 partial prior knowledge¹ regarding underlying brain activity can be used to
574 find more plausible multivariate patterns in data. Furthermore, the proposed
575 decomposition of the interpretability of MBMs into their reproducibility and
576 representativeness explains the relationship between the influential coopera-
577 tive factors in the interpretability of brain decoding models and highlights the
578 possibility of indirect and partial evaluation of interpretability by measuring
579 these effective factors.

580 *4.2. Application in Model Evaluation*

581 Discriminative models in the framework of brain decoding provide higher
582 sensitivity and specificity than univariate analysis in hypothesis testing of
583 neuroimaging data. Although multivariate hypothesis testing is performed
584 based solely on the generalization performance of classifiers, the emergent
585 need for extracting reliable complementary information regarding the un-
586 derlying neuronal activity motivated a considerable amount of research on
587 improving and assessing the interpretability of classifiers and their associated
588 MBMs. Despite ubiquitous use, the generalization performance of classifiers
589 is not a reliable criterion for assessing the interpretability of brain decoding
590 models [53]. Therefore, considering extra criteria might be required. How-
591 ever, because of the lack of a formal definition for interpretability, different
592 characteristics of brain decoding models are considered as the main objec-
593 tive in improving their interpretability. Reproducibility [53, 54], stability
594 selection [7, 47, 69], sparsity [96], and neurophysiological plausibility [97] are
595 examples of related criteria.

596 Our definition of interpretability helped us to fill this gap by introducing
597 a new multi-objective model selection criterion as a weighted compromise be-
598 tween interpretability and generalization performance of linear models. Our
599 experimental results on single-subject decoding showed that adopting the
600 new criterion for optimizing the hyper-parameters of brain decoding models
601 is an important step toward reliable visualization of learned models from
602 neuroimaging data. It is not the first time in the neuroimaging context that
603 a new metric is proposed in combination with generalization performance for
604 the model selection. Several recent studies proposed the combination of the
605 reproducibility of the maps [53, 54, 43] or the stability of the classifiers [56, 57]

¹The partial knowledge can be based on already known facts regarding the timing and location of neural activity.

606 with the performance of discriminative models to enhance the interpretability
607 of decoding models. Our definition of interpretability supports the claim that
608 the reproducibility is not the only effective factor in interpretability. There-
609 fore, our contribution can be considered a complementary effort with respect
610 to the state of the art of improving the interpretability of brain decoding at
611 the model selection level.

612 Furthermore, this work presents an effective approach for evaluating the
613 quality of different regularization strategies for improving the interpretability
614 of MBMs. As briefly reviewed in Section 1, there is a trend in research within
615 the brain decoding context in which prior knowledge is injected into the pe-
616 nalization term as a technique to improve the interpretability of decoding
617 models. Thus far, in the literature, there is no ad-hoc method to compare
618 these different methods. Our findings provide a further step toward direct
619 evaluation of interpretability of the currently proposed penalization strate-
620 gies. Such an evaluation can highlight the advantages and disadvantages of
621 applying different strategies on different data types and facilitates the choice
622 of appropriate methods for a certain application.

623 *4.3. Regularization and Interpretability*

624 Haufe et al. [39] demonstrated that the weight in linear discriminative
625 models are unable to accurately assess the relationship between indepen-
626 dent variables, primarily because of the contribution of noise in the decoding
627 process. The problem is primarily caused by the decoding process that min-
628 imizes the classification error only considering the uncertainty in the output
629 space [80, 98, 99] and not the uncertainty in the input space (or noise). The
630 authors concluded that the interpretability of brain decoding cannot be im-
631 proved using regularization. Our experimental results on the toy data (see
632 Section 3.1) shows that if the right criterion is used for selecting the best val-
633 ues for hyper-parameters, appropriate choice of the regularization strategy
634 can still play significant role in improving the interpretability of results. For
635 example, in this case, the true generative function behind the sampled data
636 is sparse (see Section 2.6.1), but because of the noise in the data, the sparse
637 model is not the most accurate one. Using a more comprehensive criterion
638 (in this case, ζ_Φ) shows the advantage of selecting correct prior assump-
639 tions about the distribution of the data via regularization. This observation
640 encourages the modification of the conclusion in [39] as follows: if the per-
641 formance of the model is the only criterion in the model selection, then the
642 interpretability cannot necessarily be improved by means of regularization.

643 *4.4. Advantage over Mass-Univariate Analysis*

644 Mass-univariate hypothesis testing methods are among the most popular
645 tools in neuroscience research because they provide significance checks and
646 a fair level of interpretability via univariate brain maps. Mass-univariate
647 analyses consist of univariate statistical tests on single independent variables
648 followed by multiple comparison correction. Generally, multiple compari-
649 son correction reduces the sensitivity of mass-univariate approaches because
650 of the large number of univariate tests involved. Cluster-based permuta-
651 tion testing [5] provides a more sensitive univariate analysis framework by
652 making the cluster assumption in the multiple comparison correction. Un-
653 fortunately, this method is not able to detect narrow spatio-temporal effects
654 in the data [2]. As a remedy, brain decoding provides a very sensitive tool
655 for hypothesis testing; it has the ability to detect multivariate patterns, but
656 suffers from a low level of interpretability. Our study proposes a possible
657 solution for the interpretability problem of classifiers, and therefore, it facili-
658 tates the application of brain decoding in the analysis of neuroimaging data.
659 Our experimental results for the MEG data demonstrate that, although the
660 non-parametric cluster-based permutation test is unable to detect the N170
661 effect in MEG data, employing ζ_Φ instead of δ_Φ in model selection not only
662 detects the stimuli-relevant information in the data, but also assures both
663 reproducible and representative spatio-temporal mapping of the timing and
664 the location of underlying neurophysiological effect.

665 *4.5. Limitations and Future Directions*

666 Despite theoretical and practical advantages, the proposed definition and
667 quantification of interpretability suffer from some limitations. All of the
668 presented concepts are defined for linear models, with the main assumption
669 that $\Phi^* \in \mathcal{H}$ (where \mathcal{H} is a class of linear functions). This fact highlights
670 the importance of linearizing the experimental protocol in the data collection
671 phase [27]. Extending the definition of interpretability to non-linear models
672 demands future research into the visualization of non-linear models in the
673 form of brain maps. Currently, our findings cannot be directly applied to
674 non-linear models. Furthermore, the proposed heuristic for the time-domain
675 MEG data applies only to binary classification. One possible solution in mul-
676 ticlass classification is to separate the decoding problem into several binary
677 sub-problems. In addition the quality of the proposed heuristic is limited for
678 the small sample size datasets (see supplementary material). Finding phys-

679 iologically relevant heuristics for other acquisition modalities such as fMRI
680 can be also considered in future work.

681 5. Conclusions

682 We presented a novel theoretical definition for the interpretability of linear
683 brain decoding and associated multivariate brain maps. We demonstrated
684 how the interpretability relates to the representativeness and reproducibility
685 of brain decoding. Although it is theoretical, the presented definition pro-
686 vides a first step toward practical solution for filling the knowledge extraction
687 gap in linear brain decoding. As an example of this major breakthrough,
688 and to provide a proof of concept, a heuristic approach based on the contrast
689 event-related field is proposed for practical evaluation of the interpretability
690 in time-domain MEG decoding. We experimentally showed that adding the
691 interpretability of brain decoding models as a criterion in the model selec-
692 tion procedure yields significantly higher interpretable models by sacrificing
693 a negligible amount of performance. Our methodological and experimental
694 achievements can be considered a complementary theoretical and practical
695 effort that contributes to researches on enhancing the interpretability of mul-
696 tivariate pattern analysis.

697 Acknowledgments

698 The author wishes to thank Sandro Vega-Pons and Nathan Weisz for
699 valuable discussions and comments.

700 Appendix A. cERF and its Generative Nature

701 According to [39], for a linear discriminative model with parameters Θ ,
702 the unique equivalent generative model can be computed as follows:

$$A \propto \Sigma_{\mathbf{X}} \Theta \quad (\text{A.1})$$

703 In a binary ($\mathbf{Y} = \{1, -1\}$) least squares classification scenario, we have:

$$A \propto \Sigma_{\mathbf{X}} \Sigma_{\mathbf{X}}^{-1} \mathbf{X}^T \mathbf{Y} = \mathbf{X}^T \mathbf{Y} = \mu^+ - \mu^- \quad (\text{A.2})$$

704 where $\Sigma_{\mathbf{X}}$ represents the covariance of the input matrix \mathbf{X} , and μ^+ and μ^-
705 are the means of positive and negative samples, respectively. Therefore,

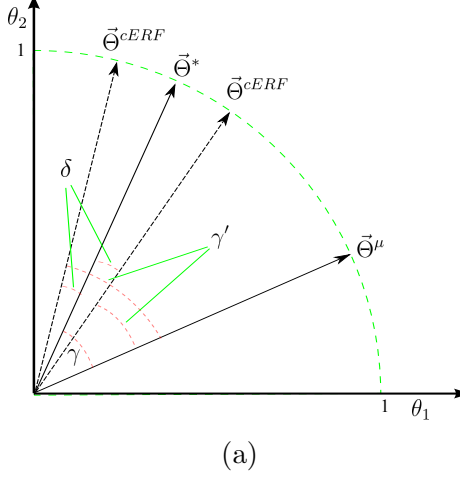


Figure B.8: Misrepresentation of $\vec{\Theta}^{cERF}$ with respect to $\vec{\Theta}^*$.

706 the equivalent generative model for the above classification problem can be
 707 derived by computing the difference between the mean of samples in two
 708 classes that is equivalent to the definition of cERF in time-domain MEG
 709 data.

710 **Appendix B. Relation between β_Φ and $\tilde{\beta}_\Phi$ (Eq. 10)**

711 Let γ be the angle between $\vec{\Theta}^\mu$ and $\vec{\Theta}^*$. Let γ' be the angle between $\vec{\Theta}^\mu$
 712 and $\vec{\Theta}^{cERF}$. Furthermore, assume that δ is the angle between $\vec{\Theta}^*$ and $\vec{\Theta}^{cERF}$
 713 and that $\Delta_\beta = \cos(\delta)$. We consider both cases in which β_Φ is underesti-
 714 mated/overestimated by $\tilde{\beta}_\Phi$ (see Figure B.8 as an example in 2-dimensional
 715 space). Then, we have:

$$\begin{aligned} \gamma &= \gamma' \pm \delta \Rightarrow \cos(\gamma) = \cos(\gamma' \pm \delta) \\ &= \cos(\gamma) \cos(\delta) \pm \sin(\gamma) \sin(\delta) = \tilde{\beta}_\Phi \Delta_\beta \pm \sqrt{(1 - \tilde{\beta}^2)(1 - \Delta_\beta^2)} \end{aligned} \quad (\text{B.1})$$

716 **Appendix C. Relation between η_Φ and $\tilde{\eta}_\Phi$ (Eq. 12)**

717 Let $\alpha_1, \dots, \alpha_m$ be the angles between $\vec{\Theta}^1, \dots, \vec{\Theta}^m$ and $\vec{\Theta}^*$, and $\gamma_1, \dots, \gamma_m$
 718 be the angles between $\vec{\Theta}^1, \dots, \vec{\Theta}^m$ and $\vec{\Theta}^{cERF}$. Furthermore, assume that

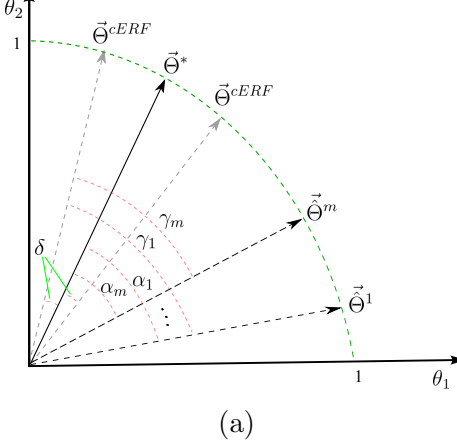


Figure C.9: Relation between η_Φ and $\tilde{\eta}_\Phi$.

719 δ is the angle between $\vec{\Theta}^*$ and $\vec{\Theta}^{cERF}$. We consider both cases in which
 720 η_Φ is underestimated/overestimated by $\tilde{\eta}_\Phi$ (see Figure C.9 as an example in
 721 2-dimensional space).

$$\begin{aligned}
 \eta_\Phi &= \frac{\cos(\alpha_1) + \cdots + \cos(\alpha_m)}{m} = \frac{\cos(\gamma_1 \pm \delta) + \cdots + \cos(\gamma_m \pm \delta)}{m} \\
 &= \frac{\cos(\gamma_1) \cos(\delta) \pm \sin(\gamma_1) \sin(\delta) + \cdots + \cos(\gamma_m) \cos(\delta) \pm \sin(\gamma_m) \sin(\delta)}{m} \\
 &\xrightarrow{\Delta_\beta = \cos(\delta)} \frac{\Delta_\beta [\cos(\gamma_1) + \cdots + \cos(\gamma_m)] \pm \sin(\delta) [\sin(\gamma_1) + \cdots + \sin(\gamma_m)]}{m} \\
 \tilde{\eta}_\Phi &\xrightarrow{\tilde{\eta}_\Phi = \frac{\cos(\gamma_1) + \cdots + \cos(\gamma_m)}{m}} \eta_\Phi = \Delta_\beta \tilde{\eta}_\Phi \pm \frac{\sqrt{1 - \Delta_\beta^2}}{m} (\sin(\gamma_1) + \cdots + \sin(\gamma_m))
 \end{aligned} \tag{C.1}$$

722 **Appendix D. Proof of Proposition 1**

723 Throughout this proof, we assume that all of the parameter vectors are
 724 normalized in the unit hypersphere (see Figure D.10 as an illustrative ex-
 725 ample in 2 dimensions). Let $T = \{\vec{\Theta}^1, \dots, \vec{\Theta}^m\}$ be a set m MBMs, for
 726 m perturbed training sets where $\vec{\Theta}^i \in \mathbb{R}^p$. Now, consider any arbitrary
 727 $p - 1$ -dimensional hyperplane \mathcal{A} that contains $\vec{\Theta}^\mu$. Clearly, \mathcal{A} divides the
 728 p -dimensional parameter space into 2 subspaces. Let ∇ and ∇ be binary

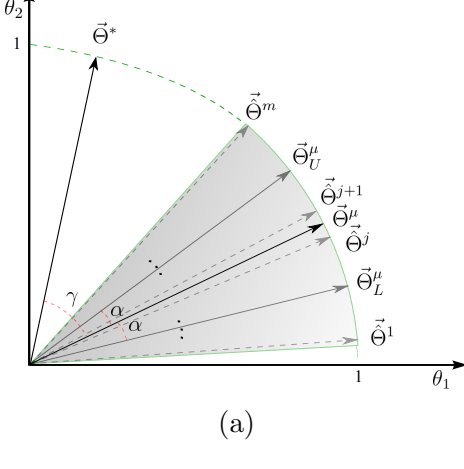
729 operators where $\vec{\Theta}^i \nabla \vec{\Theta}^k$ indicates that $\vec{\Theta}^i$ and $\vec{\Theta}^k$ are in the same subspace,
730 and $\vec{\Theta}^i \blacktriangledown \vec{\Theta}^k$ indicates that they are in different subspaces. Now, we define
731 $T_U = \{\vec{\Theta}^i \mid \vec{\Theta}^i \nabla \vec{\Theta}^*\}$ and $T_L = \{\vec{\Theta}^i \mid \vec{\Theta}^i \blacktriangledown \vec{\Theta}^*\}$. Let the cardinality of T_L
732 denoted by $n(T_L)$ be j ($n(T_L) = j$). Thus, $n(T_U) = m - j$. Now, assume that
733 $\angle(\vec{\Theta}^i, \mathcal{A}) = \alpha_1, \dots, \alpha_j$ are the angles between $\vec{\Theta}^i \in T_L$ and \mathcal{A} , and (similarly)
734 $\alpha_{j+1}, \dots, \alpha_m$ for $\vec{\Theta}^i \in T_U$ and \mathcal{A} . Based on Eq. 5, let $\vec{\Theta}_L^\mu$ and $\vec{\Theta}_U^\mu$ be the main
735 maps of T_L and T_U , respectively. Therefore, we obtain $\vec{\Theta}^\mu = \frac{\vec{\Theta}_L^\mu + \vec{\Theta}_U^\mu}{\|\vec{\Theta}_L^\mu + \vec{\Theta}_U^\mu\|}$ and
736 $\angle(\vec{\Theta}_L^\mu, \mathcal{A}) = \angle(\vec{\Theta}_U^\mu, \mathcal{A}) = \alpha$. Furthermore, assume $\angle(\vec{\Theta}^*, \mathcal{A}) = \gamma$. As a re-
737 sult, $\psi_\Phi = \cos(\alpha)$ and $\beta_\Phi = \cos(\gamma)$. According to Eq. 4 and using a cosine
738 similarity definition, we have:

$$\begin{aligned}
\eta_\Phi &= \frac{1}{m} \sum_{j=1}^m \left| \vec{\Theta}^* \cdot \vec{\Theta}^j \right| \\
&= \frac{\cos(\gamma + \alpha_1) + \dots + \cos(\gamma + \alpha_j) + \cos(\gamma - \alpha_{j+1}) + \dots + \cos(\gamma - \alpha_m)}{m} \\
&= \frac{\cos(\gamma + \alpha) + \cos(\gamma - \alpha)}{2} \\
&= \frac{\cos(\gamma) \cos(\alpha) - \sin(\gamma) \sin(\alpha) + \cos(\gamma) \cos(\alpha) + \sin(\gamma) \sin(\alpha)}{2} \\
&= \cos(\gamma) \cos(\alpha) = \beta_\Phi \times \psi_\Phi.
\end{aligned} \tag{D.1}$$

739 A similar procedure can be used to prove $\tilde{\eta}_\Phi = \tilde{\beta}_\Phi \times \psi_\Phi$ by replacing $\vec{\Theta}^*$
740 with $\vec{\Theta}^{cERF}$.

741 **Appendix E. Computing the Bias and Variance in Binary Classi-
742 fication**

743 Here, using the out-of-bag (OOB) technique, and based on procedures
744 proposed by [83] and [100], we compute the expected prediction error (EPE)
745 for a linear binary classifier Φ under bootstrap perturbation of the training
746 set. Let m be the number of perturbed training sets resulting from partition-
747 ing (X, Y) into (X_{tr}, Y_{tr}) and (X_{ts}, Y_{ts}) , i.e., training and test sets. If $\hat{\Phi}^j$ is
748 the linear classifier estimated from the j th perturbed training set, then the
749 main prediction $\Phi^\mu(\mathbf{x}_i)$ for each sample in the dataset can be computed as
750 follows:



(a)

Figure D.10: Relation between representativeness, reproducibility, and interpretability in 2 dimensions.

$$\Phi^\mu(\mathbf{x}_i) = \begin{cases} 1 & \text{if } \frac{1}{k_i} \sum_{j=1}^{k_i} \hat{\Phi}^j(\mathbf{x}_i) \geq \frac{1}{2} \\ 0 & \text{otherwise} \end{cases} \quad (\text{E.1})$$

751 where k_i is the number of times that x_i is present in the test set¹.1

752 The computation of bias is challenging because the optimal model Φ^*
753 is unknown. According to [101], misclassification error is one of the loss
754 measures that satisfies a Pythagorean-type equality, and:

$$\frac{1}{n} \sum_{i=1}^n \mathcal{L}(\Phi^\mu(\mathbf{x}_i), \Phi^*(\mathbf{x}_i)) = \frac{1}{n} \sum_{i=1}^n \mathcal{L}(y_i, \Phi^\mu(\mathbf{x}_i)) - \frac{1}{n} \sum_{i=1}^n \mathcal{L}(y_i, \Phi^*(\mathbf{x}_i)) \quad (\text{E.2})$$

755 Because all terms of the above equation are positive, the mean loss be-
756 tween the main prediction and the actual labels can be considered as an
757 upper-bound for the bias:

$$\frac{1}{n} \sum_{i=1}^n \mathcal{L}(\Phi^\mu(\mathbf{x}_i), \Phi^*(\mathbf{x}_i)) \leq \frac{1}{n} \sum_{i=1}^n \mathcal{L}(y_i, \Phi^\mu(\mathbf{x}_i)) \quad (\text{E.3})$$

¹It is expected that each sample $\mathbf{x}_i \in X$ appears (on average) $k_i \approx \frac{m}{3}$ times in the test sets.

758 Therefore, a pessimistic approximation of bias $B(\mathbf{x}_i)$ can be calculated as
 759 follows:

$$B(\mathbf{x}_i) = \begin{cases} 0 & \text{if } \Phi^\mu(\mathbf{x}_i) = y_i \\ 1 & \text{otherwise} \end{cases} \quad (\text{E.4})$$

760 Then, the unbiased and biased variances (see [83] for definitions) in each
 761 training set can be calculated by:

$$V_u^j(\mathbf{x}_i) = \begin{cases} 1 & \text{if } B(\mathbf{x}_i) = 0 \text{ and } \Phi^\mu(\mathbf{x}_i) \neq \hat{\Phi}^j(\mathbf{x}_i) \\ 0 & \text{otherwise} \end{cases} \quad (\text{E.5})$$

$$V_b^j(\mathbf{x}_i) = \begin{cases} 1 & \text{if } B(\mathbf{x}_i) = 1 \text{ and } \Phi^\mu(\mathbf{x}_i) \neq \hat{\Phi}^j(\mathbf{x}_i) \\ 0 & \text{otherwise} \end{cases} \quad (\text{E.6})$$

762 Then, the expected prediction error of Φ can be computed as follows
 763 (ignoring the irreducible error):

$$EPE_\Phi(X) = \underbrace{\frac{1}{n} \sum_{i=1}^n B(\mathbf{x}_i)}_{\text{Bias}} + \underbrace{\frac{1}{nm} \sum_{j=1}^m \sum_{i=1}^n [V_u^j(\mathbf{x}_i) - V_b^j(\mathbf{x}_i)]}_{\text{Variance}} \quad (\text{E.7})$$

764 **References**

765 [1] E. Crivellato, D. Ribatti, Soul, mind, brain: Greek philosophy and the birth
 766 of neuroscience, *Brain research bulletin* 71 (2007) 327–336.

767 [2] D. M. Groppe, T. P. Urbach, M. Kutas, Mass univariate analysis of event-
 768 related brain potentials/fields i: A critical tutorial review, *Psychophysiology*
 769 48 (2011) 1711–1725.

770 [3] E. Maris, Statistical testing in electrophysiological studies, *Psychophysiology*
 771 49 (2012) 549–565.

772 [4] E. Bullmore, M. Brammer, S. C. Williams, S. Rabe-Hesketh, N. Janot,
773 A. David, J. Mellers, R. Howard, P. Sham, Statistical methods of esti-
774 mation and inference for functional mr image analysis, *Magnetic Resonance*
775 in *Medicine* 35 (1996) 261–277.

776 [5] E. Maris, R. Oostenveld, Nonparametric statistical testing of eeg-and meg-
777 data, *Journal of neuroscience methods* 164 (2007) 177–190.

778 [6] D. M. Groppe, T. P. Urbach, M. Kutas, Mass univariate analysis of event-
779 related brain potentials/fields ii: Simulation studies, *Psychophysiology* 48
780 (2011) 1726–1737.

781 [7] M. van Gerven, C. Hesse, O. Jensen, T. Heskes, Interpreting single trial data
782 using groupwise regularisation, *NeuroImage* 46 (2009) 665–676.

783 [8] T. Davis, K. F. LaRocque, J. A. Mumford, K. A. Norman, A. D. Wagner,
784 R. A. Poldrack, What do differences between multi-voxel and univariate
785 analysis mean? how subject-, voxel-, and trial-level variance impact fmri
786 analysis, *NeuroImage* 97 (2014) 271–283.

787 [9] J.-D. Haynes, G. Rees, Decoding mental states from brain activity in hu-
788 mans, *Nature Reviews Neuroscience* 7 (2006) 523–534.

789 [10] J. R. Wolpaw, N. Birbaumer, D. J. McFarland, G. Pfurtscheller, T. M.
790 Vaughan, Brain–computer interfaces for communication and control, *Clini-
791 cal neurophysiology* 113 (2002) 767–791.

792 [11] L. F. Nicolas-Alonso, J. Gomez-Gil, Brain computer interfaces, a review,
793 *Sensors* 12 (2012) 1211–1279.

794 [12] D. Bzdok, Classical statistics and statistical learning in imaging neuro-
795 science, *arXiv preprint arXiv:1603.01857* (2016).

796 [13] F. Pereira, T. Mitchell, M. Botvinick, Machine learning classifiers and fMRI:
797 a tutorial overview., *NeuroImage* 45 (2009) 199–209.

798 [14] S. Lemm, B. Blankertz, T. Dickhaus, K.-R. Müller, Introduction to machine
799 learning for brain imaging, *Neuroimage* 56 (2011) 387–399.

800 [15] M. Besserve, K. Jerbi, F. Laurent, S. Baillet, J. Martinerie, L. Garnero,
801 Classification methods for ongoing eeg and meg signals, *Biological research*
802 40 (2007) 415–437.

803 [16] J. V. Haxby, M. I. Gobbini, M. L. Furey, A. Ishai, J. L. Schouten, P. Pietrini,
804 Distributed and Overlapping Representations of Faces and Objects in Ven-
805 tral Temporal Cortex, *Science* 293 (2001) 2425–2430.

806 [17] D. D. Cox, R. L. Savoy, Functional magnetic resonance imaging (fmri)brain
807 reading: detecting and classifying distributed patterns of fmri activity in
808 human visual cortex, *Neuroimage* 19 (2003) 261–270.

809 [18] T. M. Mitchell, R. Hutchinson, R. S. Niculescu, F. Pereira, X. Wang, M. Just,
810 S. Newman, Learning to decode cognitive states from brain images, *Machine
811 Learning* 57 (2004) 145–175.

812 [19] K. A. Norman, S. M. Polyn, G. J. Detre, J. V. Haxby, Beyond mind-reading:
813 multi-voxel pattern analysis of fmri data, *Trends in cognitive sciences* 10
814 (2006) 424–430.

815 [20] L. Parra, C. Alvino, A. Tang, B. Pearlmutter, N. Yeung, A. Osman, P. Sajda,
816 Single-trial detection in EEG and MEG: Keeping it linear, *Neurocomputing*
817 52-54 (2003) 177–183.

818 [21] J. W. Rieger, C. Reichert, K. R. Gegenfurtner, T. Noesselt, C. Braun, H.-J.
819 Heinze, R. Kruse, H. Hinrichs, Predicting the recognition of natural scenes
820 from single trial meg recordings of brain activity, *Neuroimage* 42 (2008)
821 1056–1068.

822 [22] M. K. Carroll, G. A. Cecchi, I. Rish, R. Garg, A. R. Rao, Prediction and
823 interpretation of distributed neural activity with sparse models, *NeuroImage*
824 44 (2009) 112–122.

825 [23] A. M. Chan, E. Halgren, K. Marinkovic, S. S. Cash, Decoding word and
826 category-specific spatiotemporal representations from meg and eeg, *Neu-
827 roimage* 54 (2011) 3028–3039.

828 [24] H. Huttunen, T. Manninen, J.-P. Kauppi, J. Tohka, Mind reading with
829 regularized multinomial logistic regression, *Machine vision and applications*
830 24 (2013) 1311–1325.

831 [25] D. Vidaurre, C. Bielza, P. Larrañaga, A survey of l1 regression, *International
832 Statistical Review* 81 (2013) 361–387.

833 [26] M. Abadi, R. Subramanian, S. Kia, P. Avesani, I. Patras, N. Sebe, Decaf:
834 Meg-based multimodal database for decoding affective physiological re-
835 sponses, *IEEE Transactions on Affective Computing* 6 (2015) 209–222.

836 [27] T. Naselaris, K. N. Kay, S. Nishimoto, J. L. Gallant, Encoding and decoding
837 in fmri, *Neuroimage* 56 (2011) 400–410.

838 [28] S. Weichwald, T. Meyer, O. Özdenizci, B. Schölkopf, T. Ball, M. Grosse-
839 Wentrup, Causal interpretation rules for encoding and decoding models in
840 neuroimaging, *NeuroImage* 110 (2015) 48–59.

841 [29] N. Kriegeskorte, R. Goebel, P. Bandettini, Information-based functional
842 brain mapping, *Proceedings of the National Academy of Sciences of the
843 United States of America* 103 (2006) 3863–3868.

844 [30] F. J. Valverde-Albacete, C. Peláez-Moreno, 100% classification accuracy
845 considered harmful: The normalized information transfer factor explains
846 the accuracy paradox, *PLOS ONE* 9 (2014) e84217.

847 [31] A. Ramdas, A. Singh, L. Wasserman, Classification accuracy as a proxy for
848 two sample testing, *arXiv preprint arXiv:1602.02210* (2016).

849 [32] R. Turner, A model explanation system, 2015.

850 [33] D. Baehrens, T. Schroeter, S. Harmeling, M. Kawanabe, K. Hansen, K.-R.
851 Müller, How to explain individual classification decisions, *The Journal of
852 Machine Learning Research* 11 (2010) 1803–1831.

853 [34] A. Vellido, J. Martin-Guerrero, P. Lisboa, Making machine learning models
854 interpretable, in: *Proceedings of the 20th European Symposium on Arti-
855 ficial Neural Networks, Computational Intelligence and Machine Learning
856 (ESANN)*. Bruges, Belgium, 2012, pp. 163–172.

857 [35] S. Bach, A. Binder, G. Montavon, F. Klauschen, K.-R. Müller, W. Samek,
858 On pixel-wise explanations for non-linear classifier decisions by layer-wise
859 relevance propagation, *PloS one* 10 (2015).

860 [36] G. Montavon, M. Braun, T. Krueger, K.-R. Muller, Analyzing local struc-
861 ture in kernel-based learning: Explanation, complexity, and reliability as-
862 sessment, *Signal Processing Magazine, IEEE* 30 (2013) 62–74.

863 [37] D. Yu, S. J. Lee, W. J. Lee, S. C. Kim, J. Lim, S. W. Kwon, Classification
864 of spectral data using fused lasso logistic regression, *Chemometrics and
865 Intelligent Laboratory Systems* 142 (2015) 70–77.

866 [38] K. Hansen, D. Baehrens, T. Schroeter, M. Rupp, K.-R. Müller, Visual
867 interpretation of kernel-based prediction models, *Molecular Informatics* 30
868 (2011) 817–826.

869 [39] S. Haufe, F. Meinecke, K. Görzen, S. Dähne, J.-D. Haynes, B. Blankertz,
870 F. Bießmann, On the interpretation of weight vectors of linear models in
871 multivariate neuroimaging, *NeuroImage* (2013).

872 [40] M. R. Sabuncu, A universal and efficient method to compute maps from
873 image-based prediction models, *Medical Image Computing and Computer-
874 Assisted Intervention–MICCAI 2014* (2014) 353–360.

875 [41] J.-D. Haynes, A primer on pattern-based approaches to fmri: Principles,
876 pitfalls, and perspectives, *Neuron* 87 (2015) 257–270.

877 [42] T. Naselaris, K. N. Kay, Resolving ambiguities of mvpa using explicit models
878 of representation, *Trends in cognitive sciences* 19 (2015) 551–554.

879 [43] S. C. Strother, P. M. Rasmussen, N. W. Churchill, K. Hansen, *Stability and
880 Reproducibility in fMRI Analysis*, New York: Springer-Verlag, 2014.

881 [44] A. Anderson, J. S. Labus, E. P. Vianna, E. A. Mayer, M. S. Cohen, Common
882 component classification: What can we learn from machine learning?,
883 *Neuroimage* 56 (2011) 517–524.

884 [45] K. H. Brodersen, F. Haiss, C. S. Ong, F. Jung, M. Tittgemeyer, J. M.
885 Buhmann, B. Weber, K. E. Stephan, Model-based feature construction for
886 multivariate decoding, *NeuroImage* 56 (2011) 601–615.

887 [46] G. Langs, B. H. Menze, D. Lashkari, P. Golland, Detecting stable distributed
888 patterns of brain activation using gini contrast, *NeuroImage* 56 (2011) 497–
889 507.

890 [47] G. Varoquaux, A. Gramfort, B. Thirion, Small-sample brain mapping:
891 sparse recovery on spatially correlated designs with randomization and clus-
892 tering, in: *Proceedings of the 29th International Conference on Machine
893 Learning (ICML-12)*, 2012, pp. 1375–1382.

894 [48] J.-P. Kauppi, L. Parkkonen, R. Hari, A. Hyvärinen, Decoding magnetoen-
895 cephalographic rhythmic activity using spectrospatial information, *NeuroIm-
896 age* 83 (2013) 921–936.

897 [49] S. Taulu, J. Simola, J. Nenonen, L. Parkkonen, Novel noise reduction meth-
898 ods, *Magnetoencephalography* (2014) 35–71.

899 [50] G. Varoquaux, B. Thirion, How machine learning is shaping cognitive neu-
900 roimaging, *GigaScience* 3 (2014) 28.

901 [51] E. Olivetti, S. M. Kia, P. Avesani, Meg decoding across subjects, in: Pattern
902 Recognition in Neuroimaging, 2014 International Workshop on, IEEE, 2014.

903 [52] S. Haufe, S. Dähne, V. V. Nikulin, Dimensionality reduction for the analysis
904 of brain oscillations, *NeuroImage* (2014).

905 [53] P. M. Rasmussen, L. K. Hansen, K. H. Madsen, N. W. Churchill, S. C.
906 Strother, Model sparsity and brain pattern interpretation of classification
907 models in neuroimaging, *Pattern Recognition* 45 (2012) 2085–2100.

908 [54] B. R. Conroy, J. M. Walz, P. Sajda, Fast bootstrapping and permutation
909 testing for assessing reproducibility and interpretability of multivariate fmri
910 decoding models, *PloS one* 8 (2013) e79271.

911 [55] O. Bousquet, A. Elisseeff, Stability and generalization, *The Journal of
912 Machine Learning Research* 2 (2002) 499–526.

913 [56] B. Yu, Stability, *Bernoulli* 19 (2013) 1484–1500.

914 [57] C. Lim, B. Yu, Estimation stability with cross validation (escv), *Journal of
915 Computational and Graphical Statistics* (2015).

916 [58] N. Mørch, L. K. Hansen, S. C. Strother, C. Svarer, D. A. Rottenberg,
917 B. Lautrup, R. Savoy, O. B. Paulson, Nonlinear versus linear models in
918 functional neuroimaging: Learning curves and generalization crossover, in: *Information
919 processing in medical imaging*, Springer Berlin Heidelberg, 1997,
920 pp. 259–270.

921 [59] M. Yuan, Y. Lin, Model selection and estimation in regression with grouped
922 variables, *Journal of the Royal Statistical Society: Series B (Statistical
923 Methodology)* 68 (2006) 49–67.

924 [60] R. Tibshirani, M. Saunders, S. Rosset, J. Zhu, K. Knight, Sparsity and
925 smoothness via the fused lasso, *Journal of the Royal Statistical Society: Series B (Statistical
926 Methodology)* 67 (2005) 91–108.

927 [61] E. P. Xing, M. Kolar, S. Kim, X. Chen, High-dimensional sparse structured
928 input-output models, with applications to gwas, *Practical Applications of
929 Sparse Modeling* (2014) 37.

930 [62] I. Rish, G. A. Cecchi, A. Lozano, A. Niculescu-Mizil, *Practical Applications
931 of Sparse Modeling*, MIT Press, 2014.

932 [63] L. Gosenick, S. Greer, B. Knutson, Interpretable classifiers for fmri improve
933 prediction of purchases, *Neural Systems and Rehabilitation Engineering*,
934 *IEEE Transactions on* 16 (2008) 539–548.

935 [64] M. de Brecht, N. Yamagishi, Combining sparseness and smoothness improves
936 classification accuracy and interpretability, *NeuroImage* 60 (2012) 1550–
937 1561.

938 [65] V. Michel, A. Gramfort, G. Varoquaux, E. Eger, B. Thirion, Total variation
939 regularization for fmri-based prediction of behavior, *Medical Imaging, IEEE*
940 *Transactions on* 30 (2011) 1328–1340.

941 [66] A. Gramfort, B. Thirion, G. Varoquaux, Identifying predictive regions from
942 fmri with tv-l1 prior, in: *Pattern Recognition in Neuroimaging (PRNI), 2013*
943 *International Workshop on*, IEEE, 2013, pp. 17–20.

944 [67] L. Gosenick, B. Klingenberg, S. Greer, J. Taylor, B. Knutson, Whole-brain
945 sparse penalized discriminant analysis for predicting choice, *NeuroImage* 47
946 (2009) S58.

947 [68] L. Gosenick, B. Klingenberg, K. Katovich, B. Knutson, J. E. Taylor, Interpretable
948 whole-brain prediction analysis with graphnet, *NeuroImage* 72
949 (2013) 304–321.

950 [69] Y. Wang, J. Zheng, S. Zhang, X. Duan, H. Chen, Randomized structural
951 sparsity via constrained block subsampling for improved sensitivity of dis-
952 criminative voxel identification, *NeuroImage* (2015).

953 [70] F. Bießmann, S. Dähne, F. C. Meinecke, B. Blankertz, K. Görzen, K.-R.
954 Müller, S. Haufe, On the interpretability of linear multivariate neuroimaging
955 analyses: filters, patterns and their relationship, in: *Proceedings of the 2nd*
956 *NIPS Workshop on Machine Learning and Interpretation in Neuroimaging*,
957 2012.

958 [71] S. Haufe, F. Meinecke, K. Görzen, S. Dahne, J.-D. Haynes, B. Blankertz,
959 F. Biessmann, Parameter interpretation, regularization and source localiza-
960 tion in multivariate linear models, in: *Pattern Recognition in Neuroimaging*,
961 *2014 International Workshop on*, IEEE, 2014, pp. 1–4.

962 [72] D. A. Engemann, A. Gramfort, Automated model selection in covariance
963 estimation and spatial whitening of meg and eeg signals, *NeuroImage* 108
964 (2015) 328–342.

965 [73] Z. Li, Y. Wang, Y. Wang, X. Wang, J. Zheng, H. Chen, A novel feature
966 selection approach for analyzing high dimensional functional mri data, arXiv
967 preprint arXiv:1506.08301 (2015).

968 [74] S. M. Kia, S. Vega-Pons, E. Olivetti, P. Avesani, Multi-task learning for
969 interpretation of brain decoding models, in: NIPS Workshop on Machine
970 Learning and Interpretation in Neuroimaging (MLINI), 2014, Springer Lecture
971 Notes on Artificial Intelligence Series, In press.

972 [75] R. Tibshirani, Regression shrinkage and selection via the lasso, *Journal of*
973 *the Royal Statistical Society. Series B (Methodological)* (1996) 267–288.

974 [76] H. Zou, T. Hastie, Regularization and variable selection via the elastic net,
975 *Journal of the Royal Statistical Society: Series B* 67 (2005) 301–320.

976 [77] R. Jenatton, J.-Y. Audibert, F. Bach, Structured variable selection with
977 sparsity-inducing norms, arXiv preprint arXiv:0904.3523 (2009).

978 [78] T. Poggio, C. Shelton, On the mathematical foundations of learning, *American*
979 *Mathematical Society* 39 (2002) 1–49.

980 [79] M. C.-K. Wu, S. V. David, J. L. Gallant, Complete functional characteri-
981 zation of sensory neurons by system identification, *Annu. Rev. Neurosci.* 29
982 (2006) 477–505.

983 [80] C. C. Aggarwal, P. S. Yu, A survey of uncertain data algorithms and appli-
984 cations, *Knowledge and Data Engineering, IEEE Transactions on* 21 (2009)
985 609–623.

986 [81] B. Efron, Bootstrap methods: another look at the jackknife, *The annals of*
987 *Statistics* (1979) 1–26.

988 [82] R. Kohavi, et al., A study of cross-validation and bootstrap for accuracy
989 estimation and model selection, in: *Ijcai*, volume 14, 1995, pp. 1137–1145.

990 [83] P. Domingos, A unified bias-variance decomposition for zero-one and squared
991 loss, *AAAI/IAAI 2000* (2000) 564–569.

992 [84] M. D. Rugg, M. G. Coles, *Electrophysiology of mind: Event-related brain*
993 *potentials and cognition.*, Oxford University Press, 1995.

994 [85] T. Hastie, R. Tibshirani, J. Friedman, *The elements of statistical learning*,
995 volume 2, Springer, 2009.

996 [86] A. Gramfort, G. Varoquaux, B. Thirion, Beyond brain reading: randomized
997 sparsity and clustering to simultaneously predict and identify, in: Machine
998 Learning and Interpretation in Neuroimaging, Springer, 2012, pp. 9–16.

999 [87] M. Caramia, P. Dell' Olmo, Multi-objective optimization, Multi-objective
1000 Management in Freight Logistics: Increasing Capacity, Service Level and
1001 Safety with Optimization Algorithms (2008) 11–36.

1002 [88] R. T. Marler, J. S. Arora, Survey of multi-objective optimization methods
1003 for engineering, Structural and multidisciplinary optimization 26 (2004)
1004 369–395.

1005 [89] R. N. Henson, D. G. Wakeman, V. Litvak, K. J. Friston, A Parametric Em-
1006 pirical Bayesian framework for the EEG/MEG inverse problem: generative
1007 models for multisubject and multimodal integration, Frontiers in Human
1008 Neuroscience 5 (2011).

1009 [90] S. Bentin, T. Allison, A. Puce, E. Perez, G. McCarthy, Electrophysiological
1010 studies of face perception in humans, Journal of cognitive neuroscience 8
1011 (1996) 551–565.

1012 [91] D. H. Wolpert, W. G. Macready, An efficient method to estimate bagging's
1013 generalization error, Machine Learning 35 (1999) 41–55.

1014 [92] L. Breiman, Random forests, Machine learning 45 (2001) 5–32.

1015 [93] V. N. Vapnik, S. Kotz, Estimation of dependences based on empirical data,
1016 volume 40, Springer-verlag New York, 1982.

1017 [94] V. Vapnik, The nature of statistical learning theory, Springer Science &
1018 Business Media, 2013.

1019 [95] R. Oostenveld, P. Fries, E. Maris, J.-M. Schoffelen, Fieldtrip: open source
1020 software for advanced analysis of meg, eeg, and invasive electrophysiological
1021 data, Computational intelligence and neuroscience 2011 (2010).

1022 [96] S. Dash, D. M. Malioutov, K. R. Varshney, Learning interpretable classifi-
1023 cation rules using sequential rowsampling, in: Acoustics, Speech and Signal
1024 Processing (ICASSP), 2015 IEEE International Conference on, IEEE, 2015,
1025 pp. 3337–3341.

1026 [97] B. Afshin-Pour, H. Soltanian-Zadeh, G.-A. Hossein-Zadeh, C. L. Grady, S. C.
1027 Strother, A mutual information-based metric for evaluation of fmri data-
1028 processing approaches, Human brain mapping 32 (2011) 699–715.

1029 [98] J. B. T. Zhang, Support vector classification with input data uncertainty,
1030 Advances in neural information processing systems 17 (2005) 161.

1031 [99] C. Tzelepis, V. Mezaris, I. Patras, Linear maximum margin classifier for
1032 learning from uncertain data, arXiv preprint arXiv:1504.03892 (2015).

1033 [100] G. Valentini, T. G. Dietterich, Bias-variance analysis of support vector
1034 machines for the development of svm-based ensemble methods, The Journal
1035 of Machine Learning Research 5 (2004) 725–775.

1036 [101] R. Tibshirani, Bias, variance and prediction error for classification rules,
1037 University of Toronto, Department of Statistics, 1996.